Mercury enrichment and Hg isotopes in CretaceousePaleogene boundary successions: Links to volcanism and palaeoenvironmental impacts

A.N. Sial [a, *], Jiubin Chen [b], L.D. Lacerda [c], R. Frei [d], V.C. Tewari [e], M.K. Pandit [f], C. Gaucher [g],

V.P. Ferreira [a], S. Cirilli [h], S. Peralta [i], C. Korte [d], J.A. Barbosa [j], N.S. Pereira [k]

[a] *NEG-LABISE, Department of Geology, Federal University of Pernambuco, Recife, PE, 50740-530, Brazil*

[b] *State Key Laboratory of Environmental Geochemistry, Institute of Geochemistry, Chinese Academy of Sciences, 46 Guanshui Road, Guiyang, 550002, China*

[c] *LABOMAR, Institute of Marine Sciences, Federal University of Ceará, Fortaleza, 60165-081, Brazil*

[d] *Department of Geosciences and Natural Resource Management, University of Copenhagen, Øster Voldgade 10, Copenhagen, 1350 and Nordic Center for Earth Evolution (NordCEE), Denmark*

[e] *Geology Department, Sikkim University, 6th Mile, Samdur, Tadong Gangtok, Sikkim, India*

[f] *Department of Geology, University of Rajasthan, Jaipur, 302004, India*

[g] *Facultad de Ciencias, Universidad de La República, Montevideo, Uruguay*

[h] *Department of Physics and Geology, University of Perugia, 06123, Perugia, Italy*

[i] *Instituto de Geología, Universidad Nacional de San Juan-CONICET, 5400, Argentina*

[j] *LAGESE, Department of Geology, Federal University of Pernambuco, Recife, 50740-530, Brazil*

[k] *Department of Biology, State University of Bahia, Campus VIII, Paulo Afonso, Brazil*

Abstract

We investigate the use of Hg as a proxy for volcanism by studying four distal and two proximal sections in relation to the Deccan volcanic center, straddling the CretaceousePaleogene (KPg) boundary at (a) Højerup (Denmark), Bottaccione and Padriciano (Italy), (b) Meghalaya and Jhilmili (India), and (c) Bajada del Jagüel (Argentina). Hg sequestration by organic matter results in constant Hg/TOC ratio and linear correlation between Hg content of the sediments and total organic carbon

(TOC). Elevated Hg concentrations that deviate from this linear relationship represent most likely true Hg anomalies and these notable Hg/TOC spikes (all TOC <1%) are found in the Meghalaya, Bottaccione and Højerup sections within the CF2 planktic foraminiferal biozone (spike I), at the KPg boundary (spike II), and within the P1a planktic foraminiferal subzone (spike III). Spike III occurs also in the Jhilmili section. No clear correlation between Hg/TOC and Al_2O_3 exists in any of the studied sections. The Hg anomalies probably result from strong volcanic episodes of the Deccan phase-2 (started 250 kyr before the KPg boundary and lasted for 750 kyr) that exhaled sulfuric aerosols, carbon dioxide and other toxic agents which reached a critical threshold, represented in true Hg enrichments in the paleoenviron- ments. The possibility that Hg enrichments resulted from anoxia scavenging on the seafloor and penetration downward into sediments is not supported in the stratigraphic record of Mo/Al ratios redox proxy. Hg isotopes were analyzed in samples from all KPg boundary sections in this study and from Bidart, France, the latter for comparison. Hg isotopes yielded δ^{202}Hg values ranging from 1 to 2‰ and Δ^{201}Hg signatures from 0 to 0.05‰ (spike II in Højerup, Bottaccione and Meghalaya KPg boundary layers) consistent with volcanic emission of Hg (0 to 2‰). The δ^{202}Hg in spike I in Meghalaya and Padriciano and spike III in Jhilmili is consistent with volcanic emission of Hg. Two samples from Bajada del Jagüel and four from Bidart, however, display isotope signals compatible with volcanic emission/chondrite Hg. The results of three other samples are characteristic for reworked sediment, soil and/or peat. Most of the data show small positive Δ^{201}Hg, in favor of long-term atmospheric transport prior to deposition, supporting a volcanic origin for the Hg. The present study broadens, therefore, the potential use of Hg as stratigraphic marker and, moreover, confirms that in the critical KPg transition, Hg was enriched in paleoenvironments at three distinct stages during the Deccan phase-2.

Cretaceous-Paleogene boundary, Chemostratigraphy, Total organic carbon, Molybdenum, Hg isotopes

1. Introduction

Volcanic emissions have the potential of injecting large amounts of Hg into the atmosphere and, therefore, contribute with a sig- nificant natural input of Hg to the atmosphere (e.g. Schuster et al., 2002; Pyle and Mather, 2003). Many studies have reported Hg enrichments in sedimentary records that are synchronous with modern (e.g. Martínez-Cortizas et al., 1999; Roos-Barraclough et al., 2002; Roos-Barraclough and Shotyk, 2003) and prehistoric volcanic events (e.g. Palinkas et al., 1996; Sial et al., 2010, 2013, 2014; Nascimento-Silva et al., 2011, 2013; Sanei et al., 2012; Grasby et al., 2013, 2015a, 2015b; Percival et al., 2015; Font et al., 2016). In contrast to most elements present in ash, Hg derived from volcanic activity is mainly in gaseous form (Hg^0), can be transported far in the atmosphere, reaching even global-scale distribution prior to deposition in terrestrial and marine environments and has a long atmospheric residence time (1e2 years). Through oxidation in the atmosphere, Hg^0 forms reactive $Hg^{þ2}$, soluble in water and, there- fore, enriched in the rain (e.g. Schroeder and Munthe, 1998; Witt et al., 2008 and references therein). Organic matter and clay min- erals scavenge Hg in the marine environment and fix it in bottom sediments on the sea floor (Grasby et al., 2015a; Percival et al., 2015). If Hg reaches an environment with low organic scavenging capacity on the surface, then $Hg^{þ2}$ remains in solution and is, even- tually, adsorbed onto clays and transported from land to sea. Therefore, high levels of Hg associated with argillaceous sediments can be explained by increased flux of volcanogenic Hg from conti- nents into the oceans. Higher Hg accumulation rates are typical and more pronounced in sediments deposited after glacial maxima, when runoff is increased, compared to sediment layers deposited before such events. This peculiarity is perhaps a phenomenon that can be observed globally as similar results have been observed in the Amazon region

77 (Santos et al., 2001), Antarctica (Vandal et al., 1993) and Europe (Martínez-Cortizas et al., 1999).
78 Biotic or abiotic reduction of Hg ^{2þ} to Hg^0 (g) limits the scavenging and biological fixation of Hg from
79 the atmosphere and, in consequence, allows Hg re-emission and higher concentration in the atmosphere
80 (Percival et al., 2015). Under reduced bioproductivity, Hg availability stops being captured by organic
81 matter which is one of the major Hg sinks (Sanei et al., 2012). A strong linear correlation between Hg
82 and total organic matter (TOC) contents in sediments and an apparent affinity of Hg for terrestrial
83 organic matter has been recognized (Outridge et al., 2007; Stern et al., 2009; Sanei et al., 2014) but the
84 importance of terrestrial versus aquatic retention of Hg is still an open question (Percival et al., 2015).
85 Increased Hg concentrations in sediments that deviate from a linear relationship between Hg and TOC
86 represent true Hg anomalies. On the other hand, Hg can be adsor- bed onto clays (Krupp, 1988). In this
87 case one would expect a covariation between Hg and Al2O3, as for example observed in some sections
88 across the KPg boundary (e.g. Sial et al., 2013). It has also been suggested that Hg emission rates can
89 be significantly enhanced in periods of large igneous province (LIP) volcanic activity when the marine
90 buffering control on Hg can be overwhelmed and thus generating Hg spikes in sediments (Sanei et al.,
91 2012; Grasby et al., 2013, 2015a; Font et al., 2016). There- fore, Hg anomalies could serve as proxy for
92 periods of extensive volcanic activities when LIPs, for example, could have released toxic quantities of
93 Hg into environment. The Hg flux to the sedimentary realm accompanying large amounts of magmatic
94 sulfur and other toxic metals released by LIPs (e.g. Deccan Traps, Callegaro et al., 2014) can provide
95 missing links between the terrestrial and ma- rine records of biota extinctions as suggested by Grasby et
96 al. (2015a). Sanei et al. (2012) related enhanced atmospheric Hg depositions at the PermianeTriassic
97 transition to catastrophic volcanic erup- tions of the Siberian Trap LIP event, followed by the
98 discontinuity of the organic Hg fixation that lead to an increased dissolved Hg flux. The
99 PermianeTriassic biotic crisis, as well as the extinction events in the late Capitanian and at the
100 Smithian/Spathian boundary in NW Pangea, has been linked to enhanced Hg deposition (Grasby et al.,

2013, 2015a, 2015b). In addition, the end-Pliensbachian extinction and Toarcian oceanic anoxic event (OAE) are probably related to LIP activities (KarooeFerrar), according to Percival et al. (2015). Acidic rain has been deemed responsible for the mass extinction associated to the KPg boundary (Hsü and McKenzie, 1985) and Hg enrichments in KPg boundary sedimentary rocks have been regarded as an evidence for this type of rain (Hildebrand and Boynton, 1989). Anomalous Hg concentrations in deposits spanning the KPg boundary in Dolenja Vas, Slovenia, likely resulted from sub-aerial volcanic activity (Palinkas et al., 1996). Subsequent work suggested a possible connection between enhanced Hg concentrations in sedimentary rocks across the KPg boundary and Deccan Traps events (Nascimento-Silva et al., 2011, 2013; Sial et al., 2013, 2014) and enabled a distinction of chemical fingerprints related to the Deccan volcanism from an impact event at the KPg boundary (Sial et al., 2014). However, these studies have not taken the mutual relationship between TOC content and Hg concentrations into account, and this precludes an evaluation on how lithological variation (organic matter-poor versus organic matter-rich sediments) was related to the reported Hg anomalies.

Post-emission or post-discharge Hg transformations may not drastically modify the isotopic composition of particulate Hg ac- cording to several authors (e.g. Foucher et al., 2009; Sonke et al., 2010; Estrade et al., 2011; Gehrke et al., 2011; Chen et al., 2012; Sun et al., 2013). When Hg transformations lead to change of Hg isotope signatures, this change tends to be constant under certain conditions (Laffont et al., 2009, 2011; Gehrke et al., 2011). Multiple Hg transformations may modify the Hg isotope signatures in un- predictable way, making difficult to trace the Hg source (Sonke and Blum, 2013). The Hg isotopic composition may help in the distinction be- tween volcanogenic and meteoritic Hg. It is not simple to precise the isotope composition of mantle-derived Hg because usually it is not entirely mantle-derived and/or because it has undergone fractionation during chemical/phase transformation at near surface regions (Bergquist and Blum, 2009). Mantle-derived Hg probably has d^{202}Hg values close to 0‰ according to Sherman et al. (2010), but Zambardi et al. (2009) have

125 reported values from 1.74‰ to 0.11‰ for gas and particulates, respectively, from an active volcano in
126 Italy. Generally, geogenic Hg does not have significant mass independent fractionation (MIF) of odd
127 Hg isotopes ($D^{201}Hg$ or $D^{199}Hg$) (Blum et al., 2014). On the other hand, Hg in most nat- ural samples
128 displays $d^{202}Hg$ values significantly different from crust and mantle values after it has undergone
129 cycling in the sur- face environment (Bergquist and Blum, 2009). Interestingly, these samples
130 commonly have significant MIF signatures as a result of photoreactions (or evaporation), with
131 generally negative $D^{201}Hg$ for surface soils, sediments and land plants, while positive $D^{201}Hg$ values
132 are observed for precipitation, aquatic organisms and at- mospheric particles (Blum et al., 2014). Hg
133 isotopes are potentially able to discriminate natural from anthropogenic Hg sources (Sonke and Blum,
134 2013).
135 2. The Deccan province and the KPg boundary event
136 Continuous advances in radiometric age dating have gradually confirmed the ties between the
137 Kalkarindji, Viluy, Siberian, Central Atlantic magmatic province, and Deccan volcanism to the Ear-
138 lyeMiddle Cambrian (Jourdan et al., 2014), end-Devonian, end- Permian, end-Triassic, and end-
139 Cretaceous mass extinctions, respectively (Keller and Kerr, 2014). In the Deccan lavas which flooded
140 the Indian subcontinent (Raja Rao et al., 1999), three phases of continental flood basalts are known
141 (e.g. Chenet et al., 2009) with a total of 6% volume erupted in phase-1 (C30neC31n), while 80% was
142 erupted in phase-2 (C29r), and 14% in phase-3 (C29n). An about 850,000 years quiescence of Deccan
143 volcanism separated Deccan phase-1 from phase-2. Phase-2, the longest lava flows in the Phanerozoic
144 (Self et al., 2008) started at 66.288 ± 0.027 Ma (UePb zircon dating; Schoene et al., 2015), preceding
145 the KPg boundary (65.968 ± 0.085 Ma; Renne et al., 2013) with around 250,000 years, encompassing
146 the age interval of the CF2 and CF1 planktic fora- minifers biozones. Deccan phase-2 ended at 500,000
147 years after the KPg boundary (65.552 ± 0.026 Ma). About 1.1 million km^3 of lavas were erupted

148 (Schoene et al., 2015). Deccan Traps eruptions have been blamed responsible for the mass extinction
149 documented in the intertrappean beds in India (e.g. McLean, 1985; Keller et al., 2011, 2012, and
150 references therein).
151 It is known that volcanic gases (e.g. CO2 and SO2) from a single eruptive event, and not the total
152 volume erupted, may cause devastating impacts on Earth's environment and life (Svensen et al., 2009;
153 Bond and Wignall, 2014). The Deccan Traps contain magmatic sulfur concentrations as high as 1900
154 ppm (Callegaro et al., 2014), much higher than in basalts from some other similarly sized igneous
155 provinces(e.g.Parana-Etendeka).Therefore, eruptions likely caused globally extensive acidic rains
156 before and during the KPg boundary, resulting in weathering and dissolution effects on land.
157 Dissolution of foraminifers (e.g. Gertsch et al., 2011) and of iron oxide minerals (bio- and detrital
158 magnetite) is may be considered as important evidence of acidification of oceans during this critical
159 period (Font et al., 2014). Punekar et al. (2014) investigated the environmental/biological effects of the
160 Deccan Traps eruptions using C and O isotopes and demonstrated that the global high-stress
161 environment prior to the KPg boundary is coeval with the Deccan eruption phase-2 in C29r. These
162 authors have also concluded that the Deccan phase 3 correlates with the delayed Danian biotic recovery
163 in C29n. Keller et al. (2016) reviewed the chronology and geographic distribution of the three Deccan
164 phases in India. It is not yet possible to precisely date the Deccan flood basalts associated with mass
165 extinction. Therefore, one cannot yet quantify the effects of volcanism and asteroid impact on the KPg
166 boundary mass extinction. In the present study, we use Hg, as tracer in order to investigate the
167 influence of distal volcanism, in worldwide chemostratigraphic profiles across the KPg boundary with
168 the overall aim to contribute to solve this problem.
169
170 **3. Study aims**

171 The present study aims at: (a) broadening the knowledge and contrasting Hg spikes (Hg/TOC) as
172 volcanogenic signals in marine sediments in sections straddling the boundary from different continents
173 to confirm the global extent of Hg loading related to the Deccan Traps volcanism, and (b) examining
174 Hg isotopes from these sites to help telling apart influence of volcanism from bolide impact
175 fingerprints in KPg events. By examining these Hg stratigraphic patterns, we investigate worldwide
176 fingerprints of Deccan erup- tions in climate change.

177 **4. Study areas**

178 Four distal KPg boundary sections relative to the Deccan Traps volcanic center (Denmark, Italy and
179 Argentina) and two proximal sections (India) are the focus of this study (Fig. 1). They represent well-
180 documented sites in the Northern Hemisphere (Højerup at Stevns Klint, Bottaccione at Gubbio and
181 Padriciano near Trieste), and in the Southern Hemisphere (Meghalaya, Jhilmili and Bajada del Jagüel).
182 Mercury chemostratigraphical data from the Højerup, Bottaccione, and Bajada del Jagüel sections are
183 found in Sial et al. (2014), who have not reported TOC% values alongside with Hg concentrations.
184 This lack of TOC data has limited the further use of the depicted Hg spikes as proxy for volcanism. No
185 Hg chemo- stratigraphy has been so far reported for the Padriciano section, a classical shallow-marine
186 carbonate platform (Trieste Karst, Italy), for Meghalaya, South Shillong Plateau (NE India) and for the
187 Jhilmili section (central India). The last two sections are located at proximal and very proximal
188 distances to the Deccan volcanic province, respectively, and are of paramount importance for the
189 assessment of Hg as fingerprint of eruptions in the period of the end-Cretaceous mass extinction.
190 In selecting sections for this study, we paid much attention to stratigraphic completeness of the
191 sedimentary successions and the geographic distribution of the sites. It is known that the sections at
192 Højerup (Stevns Klint), Bottaccione (Gubbio) and Meghalaya sections, based on the study of planktic
193 foraminiferal biozones, are likely complete. Stevns Klint is the best preserved and laterally the most
194 extensive KPg succession (UNESCO World Heritage Site, since June 2014). All foraminiferal biozones

195 are present in the uppermost Maastrichtian to lowermost Danian succession at Højerup (Rasmussen et
196 al., 2005; Surlyk et al., 2006; Thibault et al., 2015).
197 Refined magnetostratigraphy, planktic foraminiferal and calcareous nannofossil biostratigraphies are
198 available for the stratigraphic succession at Gubbio (e.g. Coccioni et al., 2010; Coccioni and Premoli
199 Silva, 2015). These authors have reported the presence of CF1, CF2 and CF3 foraminiferal biozones in
200 the uppermost Maastrichtian, encompassing the Scaglia Bianca and Scaglia Rossa formations up to the
201 KPg boundary. In the Shillong Plateau, seven successive planktic foraminiferal biozones from across
202 the KPg boundary at the Um Sohrynkew section (Meghalaya) are present (Mukhopadhyay, 2008; Pal et
203 al., 2015) and these are in stratigraphic order CF4, CF3, CF2 and CF1 in the upper Maas- trichtian part
204 and the P0 and Pa zones and P1a subzone in the lower Danian part, representing a biostratigraphically
205 continuous record across the KPg boundary. The Jhilmili intertrappean beds record the lower Danian
206 (planktic foraminifers P1a subzone; Keller et al., 2009) and represent the closest section to the Deccan
207 volcanic center.
208 In the Bajada del Jagüel section, Neuquén Basin, the CF1 biozone and the base of the Danian (P0, P1a,
209 P1b) seem to be missing (Keller et al., 2007; Pardo and Keller, 2008). The latest Maastrichtian as-
210 sociation of planktic foraminifers is composed of species which are not age-diagnostic and, therefore, it
211 is not possible to precisely pinpoint the exact biozones at this site. The absence of typical species of the
212 CF1 zone led Keller et al. (2007) to tentatively assign the latest Maastrichtian foraminifers in the
213 Bajada del Jagüel sec- tion to the CF2 zone. Typical Danian species occurring at the base of the Pa
214 zone (P. eugubina or P. longiapertura) seem to be absent.
215 Palamarczuk et al. (2002) have mentioned co-occurrence at Bajada del Jagüel section, of dinoflagellate
216 (*Senoniasphaera inornata* and *Damassadinium californicum*) and foraminifers (*Guembelitria cretacea*
217 and *Hedbergella montmouthensis*) within the KPg boundary sandstone and in foraminiferal zone Pa (*P.*
218 *eugubina*) above, suggesting that this 20 cm-thick sandstone which marks the KPg transition lies within

Zone P0. Besides, according to Palamarczuk et al. (2002), the 50 cm interval directly above the sandstone con- tains planktic foraminiferal species typical of zones Pa through P1c. An $^{40}Ar/^{39}Ar$ plateau age of 66 ± 0.5 Ma for feldspar from the KPg boundary ash bed was reported by the same author. Habib and Saeedi (2007) have recognized an abundance of *Manumiella seelandica* (dinoflagellate) immediately below the KPg boundary and stated that the global distribution of this species makes it an excellent biostratigraphic marker. Fossils of *M. seelan*dica have been reported from mid-latitude sites in Argentina (Palamarczuk and Habib, 2001; Palamarczuk et al., 2002). The pattern of magnetic susceptibility for the sedimentary rocks across the KPg boundary suggests that the section at Bajada del Jagüel is incomplete with respect to the very uppermost Maastrichtian, although the time span of interest may be as short as 40 kyr (Nañez et al., 2002). Aberhan et al. (2007) found neither a sign of the Danian planktic foraminiferal zone P0 nor impact specific trace element concentrations in the KPg boundary sandstone layer in the Bajada del Jagüel section, and concluded that this succession lacks about 100 kyr of a sedimentary depositional period. The disagreement about how much of sedimentary record is missing in the Bajada del Jagüel section can be somehow addressed and tested by comparing the episodic distribution of Hg/TOC anomalies with those in more complete sections as done here.

4.1. The Danish Basin, Stevns Klint, Denmark

The Stevns Klint (coastal cliffs) is located about 45 km south of Copenhagen, Denmark, on the island of Sjælland (Figs. 1, 2). The sediments, deposited in the Danish Basin, represent one of the most complete KPg boundary section worldwide. They exhibit a KPg boundary layer beneath a topographic overhang separating the lowermost Danian Cerithium Limestone Member from the over- lying lower Danian bryozoan limestone of the Stevns Klint For- mation (Fig. 8; Surlyk, 1997; Surlyk et al., 2006, 2013). The distinct boundary clay (Fiskeler Member) varies in thickness and is mainly around 5 cm, but up to 40 cm at Kulstirenden, in the northernmost part of the cliff, including here the so-called ‘red

243 layer' just above its base (Hart et al., 2004). There is clear evidence for shallowing in the latest
244 Maastrichtian before the KPg boundary, and for sea-water temperature fluctuations (Surlyk, 1997; Hart
245 et al., 2004; Thibault et al., 2015). The 45 m-thick succession exposed at Stevns Klint exhibits the
246 stratigraphic evolution of the Danish Basin from the latest Cretaceous, across the KPg boundary into
247 the early Paleogene. The most comprehensive stratigraphic studies of these sections are those of Surlyk
248 (1997), Rasmussen et al. (2005); Surlyk et al. (2006; 2013). At the Højerup coastal cliff section, the
249 Maastrichtian Møns Klint Formation (Sigerslev and Højerup members; Surlyk et al., 2013; Hansen and
250 Surlyk, 2014) is overlain by the lower Danian Rødvig Formation (Fiskeler and Cerithium Limestone
251 members) which in turn is covered by the lower to middle Danian Korsnæb Member of the Stevns
252 Klint Formation (Surlyk et al., 2006). The Cerithium Limestone is diachronous and becomes gradually
253 younger from the southern part of Stevns Klint towards the northern part. A hiatus including all the *P.*
254 *eugubina* zone is present at the Fiske- lereCerithium Limestone transition in the northern part of the
255 cliff but it is absent in the southern part (Rasmussen et al., 2005). Danian bryozoan limestone mounds,
256 outlined by black flint bands, formed shortly after the KPg boundary mass extinction (Lauridsen et al.,
257 2012 and references therein).
258
259 4.2. The Umbria-Marchean succession, Central Apennines, Italy
260 The Gubbio Mountains are part of the UmbriaeMarche Basin with two well-known KPg boundary
261 sections (Figs. 1, 2 and 8B). These occur in two parallel valleys, the Bottaccione Gorge and the
262 Contessa Highway. The former begins just outside the town of Gubbio and cuts through pelagic Middle
263 Jurassic to upper Eocene sedimentary rocks, including the Calcari Diasprigni, Maiolica, Marne a
264 Fucoidi formations and the Scaglia Group (Scaglia Bianca, Scaglia Rossa, Scaglia Variegata and
265 Scaglia Cinerea formations). The Bottaccione section represents the magnetostratigraphic standard for
266 the Upper CretaceouseEocene interval (e.g. Galeotti et al., 2015) and contains a 1 cm-thick clay layer at

the KPg boundary (Fig. 2) within the Scaglia Rossa Formation, enriched in Ir (Alvarez et al., 1980). In contrast to Stevns Klint, the KPg boundary layer at Gubbio has a very short lateral extent as the succession is tilted (Fig. 2B).

Alternation of gray and pink colored beds marks the contact between the Scaglia Bianca and the overlying Scaglia Rossa for- mations. The latter brackets the KPg boundary and consists of predominantly pink to red pelagic limestones with cherty nodules and calcareous marls, with bedding thicknesses between 10 and 20 cm. This Upper Cretaceous to lower middle Eocene succession represents an apparently continuous stratigraphic record across the KPg boundary and based on abundant planktic and benthic fora- minifers and calcareous nannofossils, it has been dated as Late Cretaceous to early middle Eocene (Premoli Silva and Sliter, 1994; Alvarez, 2009; Coccioni and Premoli Silva, 2015 and references therein).

The KPg boundary crops out on the eastern side of the main road and lies around 240 m above the base of the Scaglia Rossa Forma- tion (Figs. 2B, 8B). The topmost Cretaceous in this section is rep- resented by a 30e40 cm-thick whitish limestone bed, overlain by the 2 cm-thick dark clay KPg boundary layer which correlates to the well-known KPg boundary mass-extinction event (Premoli Silva and Sliter, 1994). The lowermost Paleocene is correlated with the occurrence of *Globigerina eugubina* foraminiferal zone (=*Parvorugoglobigerina eugubina*; Luterbacher and Premoli Silva, 1964).

4.3. The Trieste Karst, NW Adriatic platform, Italy

The Karst region including the Trieste area of Italy and a portion of Slovenia is part of the Adriatic platform and is characterized by Maastrichtian to Danian peritidal carbonate deposits (Fig. 3). In Italy, the thickest succession of this shallow carbonate platform is located at Padriciano (Fig. 3). In the Trieste Karst, the KPg boundary is well-documented in some sections at Padriciano (Pugliese et al., 1995, 2000; Tewari et al., 2007). The interval including the KPg boundary is characterized by presence

of several peritidal cycles consisting of basal breccias, lagoonal limestone, and stromatolitic limestone with typical fenestral fabric.

The KPg boundary in the carbonate platform of the Karst region of Slovenia was first identified by Drobne et al. (1989). The main criteria they used to identify the KPg boundary was by the occur- rence of certain biota, particularly by the disappearance of Creta-ceous taxa and appearance of Paleogene ones, by identification of foraminiferal zone SBZ1 and of magnetic polarity Ch29r, the presence of and Ir anomaly and by the strong negative shift of $\delta^{13}C$ values across the KPg boundary (Hansen et al., 1995; Marton et al., 1995; Ogorelec et al., 1995; Hansen and Toft, 1996; Palinkas et al., 1996). The same criteria have been adopted for locating the KPg boundary in the Trieste Karst and, in addition, the presence of microtektites at the top of a Maastrichtian breccia near the village of Padriciano was also regarded as evidence for the record of the KPg boundary in this region (Gregoric et al., 1998).

The peritidal shallow carbonate succession at Padriciano is represented by the Liburnia Formation (Fig. 3) which contains a Maastrichtian breccia (50 cm-thick, Fig. 2), another breccia (20 cm- thick) of dark limestone with rudist shell fragments and foramin- ifers (Tewari et al., 2007) about 80 cm below the upper breccia (Fig. 2). The KPg boundary is situated at the base of the upper breccia, the latter overlain by a succession of light gray Danian limestone with Microcodium that is overlain by stromatolitic limestone also with Microcodium. A change in the foraminifer species from Miliolidae, Rhapydionina liburnica, Fleuyriana adriatica to the occurrence of Microcodium and Bangiana hanseni is present immediately below the upper breccia (Caffau et al., 1998). This brown limestone, with gastropod fragments and Microcodium, is overlain by gray stromatolitic limestone capped or penetrated by Microcodium. Further peritidal cycles of gray limestone overlain by stromatolitic limestone with Microcodium, forming thick units, follow up-section. Within lagoonal limestones of these cycles, some Danian opportunistic and r-strategist foraminifers taxa (e.g. Bangiana hanseni and small Miliolidae) appear (Pugliese et al., 2000; Tewari et al., 2007) and characterize the Danian larger benthic

foraminiferal zone 1 (SBZ 1; Serra-Kiel et al., 1998) which corresponds to the planktic foramineral P0, Pa and P1 biozones of Berggren et al. (1995).

4.4. The Neuquén Basin, Patagonia, Argentina

The Neuquén Basin in Patagonia of western Argentina is located between 32 and 40 S latitude on the eastern side of the Andes in Argentina and central Chile. This foreland basin comprises Upper Triassic to Miocene deposits (Vergani et al., 1995; Legarreta and Uliana, 1999; Howell et al., 2005). The KPg transition is situated in the Upper Cretaceouselower Paleocene Malargüe Group that comprises the Allen, Jagüel, Roca and El Carrizo formations and depos- ited unconformably overlying the Upper Cretaceous Neuquén Group (Legarreta et al., 1989; Casadío, 1998; Heredía and Salgado, 1999). The KPg transition in this basin has been extensively investigated by biostratigraphy, microfacies analysis, bulk rock/clay mineralogy, isotope stratigraphy, and trace and major element chemistry (e.g. Howell et al., 2005; Scasso et al., 2005; Aberhan et al., 2007; Keller et al., 2007; Musso et al., 2012). These and further results show that the Maastrichtian succession was deposited during trans- gression. A regressive trend was recorded in the Paleocene (Scasso et al., 2005; Aguirre-Urreta et al., 2011). The Jagüel Formation en- compasses the KPg boundary (e.g. Uliana and Biddle, 1988) and consists of 90-m thick, monotonous marine mudstones deposited in a mid-to outer-shelf environment, covered by bioclastic marine limestones of the Danian Roca Formation (Fig. 4). The KPg boundary interval has been identified on the basis of palynomorphs (Papú et al., 1999), ostracods (Bertels, 1975), calcareous nannofossils and foraminifers (Nan~ez and Concheyro, 1997). The position of the KPg transition is constrained to a single, thin coarse-grained sandstone bed (Palamarczuk and Habib, 2001; Palamarczuk et al., 2002; Scasso et al., 2005) in the upper half of the Jagüel Formation, and Danian age above has been confirmed by calcareous nannofossils (Scasso et al., 2005). This 15e25 cm thick non to slightly lithified tuffaceous sandstone can be traced laterally for 5 km in the area. It occurs within the

339 homogeneous shelf mudstone of the Jagüel Formation and contains abundant volcanogenic plagioclase
340 volcanic lithics, shell detritus and shark teeth (Palamarczuk et al., 2002). This KPg tran- sition
341 sandstone shows abundant rip-up clasts, erosional base, coarse-grain size, normal grading and
342 hummocky cross-bedding, and has been interpreted as a tsunami deposit in a shelf environ- ment,
343 related to the Chicxulub bolide impact in Mexico (Scasso et al., 2005). Spherule, shocked quartz or
344 enrichment of meteoritic com- ponents has not been reported from this layer or the mudstones
345 immediately above. Keller et al. (2007) suggest that the KPg boundary is marked by erosional-based
346 sandstone that signifies a hiatus. This sandstone, previously interpreted as a mark of the KPg transition,
347 contains diverse planktic foraminiferal zone P1c assemblages and nanno- fossils of zone NP1b
348 immediately above (Keller et al., 2007). These authors suggested that its deposition occurred at about
349 500 kyr after the KPg hiatus.
350
351 4.5. Meghalaya, South Shillong Plateau, NE India
352 The Um Sohrynkew section is situated in northeastern India, north of Bangladesh and in a distance of
353 about 800e1000 km from the Deccan volcanic province (Figs. 5, 6 and 7). It is exposed along the Um
354 Sohrynkew River in Meghalaya, next to Therria village, East Khasi Hills District, south Shillong
355 Plateau, in the eastern Himalayas (Fig. 7). The succession comprises the most complete marine KPg
356 succession known from India, and possibly worldwide (Gertsch et al., 2011 and references therein).
357 The section displays strong evidence of mass extinction patterns (e.g. planktic foraminifers and larger
358 ammonoids), a preserved KPg boundary layer, as well as the first appearance of Danian foraminifers,
359 and indications for sea- level change (Keller et al., 2008, 2009; Tewari et al., 2010a, 2010b; Gertsch et
360 al., 2011 and references therein). The KPg boundary at Um Sohrynkew (Fig. 5) is marked by a thin red
361 clay layer enriched in Ir and other platinum group elements (Pandey, 1990; Bhandari et al., 1993, 1994;
362 Garg et al., 2006) with abundant subangular quartz grains in a brown matrix (Gertsch et al. 2011). This

363 section consists of a continuous CampanianeEocene succession characteristic of coastal, estuarine and
364 nearshore envi- ronments (Nagappa, 1959; Krishnan, 1968; Banerji, 1981; Tewari et al., 2010a, 2010b)
365 with marine shelf sediments including thick sandstone layers, marl, shale and carbonates.
366 Based on the distribution of zonal indices, Mukhopadhyay (2008) and Pal et al. (2015) have recognized
367 seven successive planktic foraminiferal zones across the KPg boundary at the Um Sohrynkew River
368 section. These zones are, in stratigraphic order, CF4, CF3, CF2 and CF1 in the upper Maastrichtian part
369 and Zone P0, Zone Pa and Subzone P1a in the lower Danian part, thus, representing a bio-
370 stratigraphically continuous succession across the KPg boundary. We focus only on 2.5 m of the
371 MaastrichtianeDanian interval of the Um Sohrynkew section, bracketing the KPg boundary. Twenty-
372 five samples have been stratigraphically collected at an interval of 10 cm: seven samples from greenish
373 sandstone and greenish gray clayey marl of the Maastrichtian Mahadeo Formation, one sample from
374 the rust-red-colored sandyesilty KPg boundary layer (about 2 cm thick) and the rest of samples from
375 the Danian Langpar For- mation whose basal portion is formed by a 10 cm-thick bioturbated sandstone
376 overlain by dark to light gray shale to marl (Fig. 5).
377
378 4.6. Jhilmili intertrappean sediments, Madhya Pradesh, Central India
379 The Deccan intertrappean sediments have been regarded for long time as terrestrial deposits,
380 Maastrichtian in age, until the work by Keller et al. (2009) who studied the sedimentology, microfacies,
381 biostratigraphy and, C- and O-isotope chemo- stratigraphy of a thick intertrappean succession next to
382 the village of Jhilmili (22°02’044” N, 79°09’034” E), Chhindwara District of Madhya Pradesh, central
383 India. This succession consists of sedi- ments with early Danian planktic foraminifera sandwiched be-
384 tween two basalt flow horizons (the lower and upper trap basalts correspond, respectively, to C29r and
385 the C29r/C29n transition) (Keller et al., 2009) and is located near the main road that links Seoni and
386 Chhindwara, exposed in a shallow-river valley. Its lithological types comprise claystones, paleosols,

387 siltstones, clayeyesilty marlstones to limestones and can be subdivided into three different units
388 summarized below.
389 The 6 m thick lowermost unit (unit 1), deposited in terrestrial and palustrine environments, overlies the
390 strongly weathered lower basalt trap. It consists of red clayey siltstone with carbonate nodules and
391 coarser quartz grains, becoming less abundant to- wards the top. The unit is overlain by another about
392 70 cm thick lacustrine-brackish deposit (unit 2), that consists of pink, reddish to yellow laminated
393 clays, containing marly limestones in its lower part, and with abundant volcanic glass shards. The top
394 of this unit is formed by coarse-grained nodular limestone that was probably deposited in fresh to
395 brackish-marine water deduced from the common freshwater and rare brackish-water ostracods along
396 with rare planktic foraminifers (Keller et al., 2009).
397 Unit 3 is similar to the unit 2, consisting of red clayey siltstones, with clay and carbonate clasts
398 interbedded with fine-sand layers. Glass spherules and shards are present as well as a carbonate- nodule
399 layer. A 1 cm-thick black charcoal layer separates this unit from the overlying basaltic flow which is
400 strongly weathered. Immediately below this upper basalt trap, a 30 cm-thick tempestite has been
401 recognized.
402 In this intertrappean succession, Keller et al. (2009) have iden- tified a thin aquatic interval of fresh
403 water ponds and lakes deposits overlain by shallow coastal marine sediments with brackish marine
404 ostracods and lower Danian zone P1a planktic foraminifers, very close to the KPg boundary. Their
405 most important contributions were: (a) discovery of environmental changes preserved within the
406 intertrappean sediments at Jhilmili and (b) a marine incursion pointing to the existence of a seaway at
407 least 800 km long, across India, from the west through the NarmadaeTapti rift valley (Shukla and
408 Srivastava, 2008; Keller et al., 2009, Fig. 6).
409
410 5. Methods

411 5.1. Analysis of total organic carbon (TOC), molybdenum and aluminum

412 All analyzed samples in this study were decarbonated using 6 M HCl prior to TOC analyses. Acid
413 remains were subsequentlyremoved by a repeated procedure of rinsing, centrifugation, and decantation
414 of supernatant liquids. Remaining fractions were weighed out again after 24 h freeze drying at
415 temperatures of 54 C. The CaCO3 concentration was calculated by the weight difference of the
416 aliquots before, and after the acid treatment. The total organic carbon was measured on 160 mg of
417 decarbonated aliquot using a Carbon-Sulfur-Determinator (Eltra CS 500) at the Department of
418 Geosciences and Natural Resources Management, University of Copenhagen. The sample was
419 combusted for 90 s in a ceramic boat at a temperature of ~1350 C with a catalytic oxidation process.
420 The resulting CO2 signal was electronically linearized and integrated, and subsequently used to
421 calculate the TOC. The reproducibility, obtained from multiple analyses of the in-house reference
422 material SKK-9 (TOC 1⁄4 6.88%), is generally better than 0.1% (1 sd).
423 Molybdenum and aluminum were analyzed by ICPeMS at the Geological Survey (GEUS) in
424 Copenhagen, Denmark after sample digestion with 6N HCl, dissolving all carbonates, but probably
425 leaving some silicate detrital material back. These analyses are, therefore, incomplete whole-rock
426 analyses and the reported aluminum concentrations are regarded as minimum-rock concen- trations.
427 Molybdenum has been measured over two different iso- topes (95Mo and 98Mo) and here the total Mo
428 concentrations are calculated from the 95Mo peak.
429

430 5.2. Analysis of mercury

431 Mercury concentrations were determined in homogenized powdered samples at the LABOMAR in the
432 Federal University of Ceará, Brazil, using the method described by Sial et al. (2014, p. 105) “glass and
433 plastic ware were decontaminated by immersion for 1 day in (10% v/v) Extran solution (MERCK),
434 followed by immersion for 2 days in diluted HCl (5% v/v) and final rinsing with Milli-Q water. All

chemical reagents used were of the least analytical grade. Cold Vapor Atomic Fluorescence Spectrophotometry, using a Millenium Merlin PSA spectrophotometer, was used for Hg determination, after Hg2þ reduction with SnCl2. All samples were analyzed in duplicates, showing reproducibility within 9.5%. A certified reference material (NIST 2702, Canada) was simulta- neously analyzed to evaluate Hg determination accuracy. Such analysis showed a precision of 4%, as indicated by the relative standard deviation of three replicates, and presented Hg recovery of 98.8± 6.2%. The Hg detection limit estimated as 3 times the standard deviation of reagent blanks was 1.26 $ng.g^{-1}$. In all cases, blank signals were lower than 0.5% of sample analysis. The con- centration values were not corrected for recoveries found in the certified material powder, following Sial et al. (2014, p. 105)."

5.3. Analysis of carbon isotopes

Inorganic and organic $\delta^{13}C$ analyses of carbonates were per- formed at the Stable Isotope Laboratory (LABISE) of the Department of Geology, Federal University of Pernambuco, Brazil. Extraction of CO_2 gas was performed using a conventional high vacuum extrac- tion line after reaction with 100% orthophosphoric acid at 25 °C for one day. Released CO_2 was analyzed in a Thermofinnigan Delta V Advantage mass spectrometer and results are reported in δ notation in permil (‰) VPDB.

$\delta^{13}Corg$ was analyzed from total organic carbon of insoluble residues of samples from all the studied sections. After whole-rock samples were crushed into powder "insoluble residues for organic carbon isotope analysis were obtained by acidifying these whole- rock powders in increasing concentrations (0.4, 0.6 and 0.8 mol l^{-1}) of H_3PO_4 for three days to dissolve all carbonate minerals. Care was taken to ensure that acid was added andacidification continued until there was absolutely no visible car- bonate dissolution so that the analyses would not be affected by contamination from residual inorganic carbon. The insoluble resi- dues were then rinsed with DI water, dried and loaded into tin capsules for isotopic analysis (Sial et al., 2014, p. 105)." $\delta^{13}C$ org was measured using continuous flow elemental analysis

isotope-ratio mass spectrometry with a Delta V Advantage mass spectrometer interfaced with a COSTECH elemental combustion system (com- bined analytical and sampling error of ±0.2‰).

5.4. Analysis of Hg isotopes

Mercury isotope ratios were determined on the new MC-ICP-MS (Nu-Plasma II, Nu Instruments) equipped with sixteen Faraday cups at the State Key Laboratory of Environmental Geochemistry, Insti- tute of Geochemistry, Chinese Academy of Sciences, China, following a method similar to Huang et al. (2015). A continuous flow cold-vapor generation system (CV) was coupled with an Ari- dus II desolvation unit (CETAC Technologies, U.S.) for Hg and Tl introduction, respectively. The instrumental baseline was measured by de-focusing before each sample and standard. Both the internal standard method and the standard-sample bracketing technique were used to correct for instrumental mass bias (Chen et al., 2010; Jiskra et al., 2012).

Mass-dependent fractionation (MDF) of Hg isotopes is reported in delta notation, δ, which is the permil (‰) deviation relative to the SRM 3133 standard. Mass independent fractionation (MIF) of Hg isotopes is reported using upper-case delta notation, Δ, which is the deviation of the measured isotope ratio from the theoretical ratio predicted by MDF. The analytical quality was controlled by repeated measurement of standard materials. Long-term analysis gave average values of -0.54 ± 0.10‰, -0.02 ± 0.04‰ and -0.04 ± 0.04‰ for δ^{202}Hg, Δ^{199}Hg and Δ^{201}Hg of UM-Almaden Hg (2SD, n = 21), and of -1.22 ± 0.16‰, 0.06 ± 0.09‰ and 0.03 ± 0.10‰ for those of Fluka Hg (2SD, n 1⁄4 13), respectively, in accordance with the published results (Bergquist and Blum, 2009; Chen et al., 2010; Chen et al., 2012; Jiskra et al., 2012). The 2SD of the isotopic compositions of the UM-Almaden were considered as the analytical uncertainty for the isotopic compositions of samples. When the uncertainty of the replicate isotopic measurements of one sample was larger than the 2SD of the UM-Almaden, the un- certainty was applied to the sample (Huang et al., 2015).

483

484 6. Results and data interpretation

485

486 6.1. Carbon-isotope chemostratigraphy and total organic carbon (TOC)

487 The covariation between carbonate and sedimentary organic C- isotope records can help establishing
488 whether variations in the δ^{13}Ccarb record reflect changes in the isotopic composition of the ancient
489 dissolved inorganic carbon pool (e.g. Oehlert and Swart, 2014, and references therein). Covariant
490 dδ^{13}Ccarb and δ^{13}Corg records evidence that both the carbonate and organic matter were originally
491 produced in the surface waters of the ocean and have retained their original δ^{13}C composition (e.g.
492 Korte and Kozur, 2010; Meyer et al., 2013) as it is believed that no secondary processes are able to
493 shift δ^{13}Ccarb and δ^{13}Corg in the same direction at the same rate (Knoll et al., 1986). Decoupled
494 δ^{13}Ccarb and δ^{13}Corg records indicate diagenetic alteration (e.g. Grotzinger et al., 2011; Meyer et al.,
495 2013) or that local syn-sedimentary processes have intro- duced noise in the δ^{13}Corg record (Maloof et
496 al., 2010). Global δ^{13}C records of bulk sediment comparing C-isotope pathways across the KPg
497 boundary from far apart sections at Højerup, Bottaccione and Bajada del Jagüel localities (Figs. 8 and
498 9), were previously published by Sial et al. (2014).
499 New δ^{13}C carb data are presented here for the sections in the Meghalaya, Jhilmili and Padriciano
500 (Tables 1 and 3; Figs. 8 and 10) and δ^{13}C org for the six sections under consideration (Tables 1e3, Figs.
501 8, 9, 10).
502 Twenty-five samples were collected stratigraphically at centi- meter scale, perpendicular to the strike of
503 the strata, from a 2.5 m section across the KPg boundary at the Um Sohrynkew River in Meghalaya
504 (Table 3; Fig. 10A). The lowermost meter in this section is composed of greenish glauconitic sandstone
505 and greenish-gray shale belonging to the Maastrichtian Mahadeo Formation, below the yellowish
506 brown-reddish KPg boundary clay layer (samples KT- 1 through KT-7 in Table 3 lie immediately

507 below the KPg boundary clay layer). Light to medium-gray and dark-gray to light-medium gray shale
508 (samples KT-8 through KT-25; Table 3) were collected from the lowermost portion of the Danian
509 Langpar Formation, immediately above the KPg boundary layer.
510 Twenty-four samples were collected from a 7.3 m section o intertrappean beds (Table 3; Fig. 10B)
511 between two basaltic flow layers in a shallow river valley next to the village of Jhilmili, Chhindwara
512 District of Madhya Pradesh. The lowermost layer in this section is composed of ferricrete paleosol with
513 calcitic veins which is covered by a hard sediment layer within paleosol with clastic grains and calcitic
514 cement. This is followed upward by fine- grained, brick red with yellowish tint soft ferricrete, and then
515 by comparably harder grayish brown claystone with laminar features. Towards the top, this section
516 contains again fine-grained, brick red soft ferricrete with yellowish tint, which is covered by a greenish
517 clay layer with calcitic veins. Eighteen samples of carbonates from the Liburnia Formation have been
518 collected from a representative section across the KPg boundary at a quarry at Padriciano in the Trieste
519 Karst (Table 1; Fig. 8C).
520 Among the six sections in this study, the three from Europe and the one from Bajada del Jagüel display
521 isotopically lighter carbonate composition immediately above the KPg boundary, portrayed by a shift
522 to lighter $\delta^{13}C$ values (Figs. 8 and 9). This picture could be partially a consequence of an increase of
523 volcanic CO_2 in the atmosphere (80% of the Deccan phase 2 eruptions took place within the time lapse
524 recorded in the sections examined) which may have accounted also for the large negative $\delta^{13}C$
525 excursion at or just below the KPg boundary. Another important factor driving this negative excursion
526 is the collapse of bioproductivity at the boundary, with a gradual recovery in the early Danian. An
527 abrupt decrease of $\delta^{13}C$ carb at the KPg boundary is noticeable at the Højerup, Bottaccione and
528 Meghalaya sections. At the Bajada del Jagüel and Padriciano localities, there is a strong decrease of
529 $\delta^{13}C$ values that predate (but very close) the KPg transition. In Jhilmili, the end-Cretaceous is
530 represented by basalt in the studied section and the $\delta^{13}C$ pathway shows a prominent minimum (-12‰)

531 at about 1 m above the lower basaltic flow, and upsection this curve gradually shows less negative
532 values, predominantly from -4 to -3‰.
533 The total organic carbon content in the studied sections, expressed as percent TOC, are <1.0% (Tables
534 1e3), with the majority of samples yielding values < 0.2%. Among the complete sections in this study,
535 the highest TOC values were recorded in the KPg boundary layer in the Højerup section (~0.9%) and in
536 the uppermost Maastrichtian and Danian portions of the Meghalaya section (0.3e0.6%), while much
537 lower TOC values are observed in the whole Bottaccione section (0.01-0.09%). At Højerup, the TOC
538 stratigraphic variation curve shows a very monotonous pattern with almost no oscillation except a
539 prominent positive shift at the KPg boundary layer (Fig. 8A). At Gubbio, however, the TOC strati-
540 graphic pathway shows vigorous oscillations with a negative shift about 4 m below the KPg boundary
541 (within the CF2 biozone), a small negative excursion at the KPg boundary and a prominent positive
542 shift about 8 m above the KPg boundary (within the P1a biozone). At Meghalaya, the TOC
543 stratigraphic variation curve shows two marked positive excursions, about one meter below the KPg
544 boundary (CF2 biozone) and another at the KPg boundary and in lowermost Danian (P0 biozone).
545 At the Padriciano section, the TOC values are all <0.3%, with highest values found in the Maastrichtian
546 portion of the section and a positive shift in the KPg boundary breccia. In Bajada del Jagüel, TOC
547 values range between 0.3 (Maastrichtian) and 0.8% (Danian), and a strong shift to values as low as
548 0.01% is the sandstone that marks the KPg transition (Table 2). At the Jhilmili section, the TOC
549 stratigraphic pathway shows vigorous oscillations in the lower half of the section, followed by a strong
550 positive shift in the upper half of this curve.
551 The δ^{13}C org curve for organic matter from the Højerup section displays a gradual decrease of values
552 from -23‰ towards the KPg boundary layer with a minimum of -27‰ at the KPg boundary (Fig. 8A).
553 This is followed by a strong increase to -22‰ upsection and again by a negative shift to -27‰ and a
554 positive shift to -22‰. At the Bottaccione section (Fig. 8B), the δ^{13}Corg curve shows a less

555 pronounced decrease towards to the KPg boundary within the CF2eCF1 biozones, a discrete decrease at
556 the KPg boundary, and two positive shifts within the P1a biozone. The Meghalaya section shows a
557 different pattern (Fig. 10A) with no decrease of δ^{13}Corg towards the KPg boundary, contrary to what
558 was observed at Højerup and Bottaccione. At the KPg boundary, the δ^{13}Corg pathway shows a
559 maximum (-21‰) within the P0 biozone, followed upsection by a monotonous variation curve within
560 the P1a (1) subzone and a small increase to -24‰ within the P1a (2) subzone. A covariance record
561 between δ^{13}Ccarb and δ^{13}Corg at the Højerup and Bottaccione sections is depicted in Fig. 8A and B,
562 providing evi- dence that the carbonate and organic matter were produced in the surface waters of the
563 ocean and have probably retained their original respective δ^{13}C composition. At Meghalaya, the
564 δ^{13}Ccarb and δ^{13}Corg curves display opposite behaviors around the KPg boundary, with large positive
565 excursion of the δ^{13}Corg curve.
566 The Padriciano section is characterized by a δ^{13}Corg curve (Fig. 8C) similar to that observed at
567 Højerup, with a gradual decrease from -21 to -23‰ from one meter below the KePg transition to the
568 KPg transition, reaching a minimum about 0.5 m above this transition, and followed upsection by a
569 positive shift. The δ^{13}C org curve for Bajada del Jagüel section exhibits a minimum (~-26‰) about 0.5
570 m below the KPg boundary (within the CF2 biozone), a negative excursion at the boundary, a positive
571 excursion (-23‰) immediately above the boundary, and a gradual and strong decrease to -26‰
572 upsection (Fig. 9). For the Danian Jhilmili section, the δ^{13}Corg shows two positive shifts within the P1a
573 biozone with a strong negative shift at the top, close to the upper basalt flow. Except for Meghalaya,
574 the behavior of the δ^{13}Corg stratigraphic variation curves for these sections may possibly be explained
575 by a response to growing deterioration of the environment at the end of the Maastrichtian with gradual
576 decrease of organic productivity, followed by its gradual recovery early in the Danian.
577

578 6.2. Mercury concentrations, Hg/TOC and Mo/Al ratios

579 Mercury concentrations for stratigraphically collected samples from Højerup, Bottaccione (Table 1)
580 and Bajada del Jagüel (Table 2) sections are available in Sial et al. (2014). The Hg variation pattern for
581 the Højerup section displays an Hg enhancement (260 ng.g^{-1}) that coincides with a minimum value of
582 $\delta^{13}C$ in the Fiskeler Member at the KPg boundary (Fig. 8A). A second Hg enrichment (48 ng.g^{-1}) is
583 seen 1.6 m above the KPg boundary layer. In the Bottaccione section, three Hg enhancements (Fig. 8B)
584 were observed by Sial et al. (2014), a small one (2 ng.g^{-1}) at about 6 m below the KPg boundary, the
585 largest one at the KPg boundary (6 ng.g^{-1}) which coincides with a minimum of $\delta^{13}C$, and a third one at
586 about 7 m above the KPg boundary (4 ng.g^{-1}). In the Hg strati- graphic variation curve for the Bajada
587 del Jagüel section (Fig. 9), three Hg enhancements are present, one at about 65 cm below the KPg
588 boundary (17 ng.g^{-1}Hg), a second one at this boundary (16 ng.g^{-1}) and a third one (13 ng.g^{-1}) around 15
589 cm above that.
590 Hg concentrations were measured in eighteen bulk samples from Padriciano (Table 1), twenty-five
591 from Meghalaya and eigh- teen from Jhilmili (Table 3) and the corresponding Hg variation patterns are
592 shown in Figs. 8C, 10A and B. In Meghalaya, an Hg enrichment is seen at about 0.5 m below the KPg
593 boundary layer (Fig. 10A), preceding the prominent negative $\delta^{13}C$ that marks the KPg boundary. Two
594 prominent Hg enrichments are present in the intertrappean Danian sediments of the Jhilmili section. In
595 the Padriciano section, the Hg stratigraphic variation pathway shows a prominent Hg enrichment (183
596 ng.g^{-1}) at about 40 cm below the KPg boundary, followed by a second Hg enrichment (51 ng.g^{-1}) at
597 about 25 cm above the KPg boundary and a more discrete one (31 ng.g^{-1}; Fig. 9C) at about 2.40 m
598 above the KPg boundary.
599 In order to screen for Hg enrichments in these sections that represent true Hg loading to the
600 environment, Hg concentrations have been normalized to corresponding TOC values following the
601 approach recommended by Grasby et al. (2015a, 2015b) and Percival et al. (2015). However, in
602 normalizing Hg concentrations to TOC, caution should be taken in using Hg-TOC pairs in which TOC

603 concentrations are <0.2% because too low Hg concentrations may produce, in some cases, unrealistic
604 or even false Hg/TOC spikes.
605 Absolute Hg concentrations, TOC, Hg/TOC and Mo/Al ratios for all the studied sections are listed in
606 Tables 1e3 and are plotted in Figs. 8Ae10B. In most cases, elevated Hg concentrations, after
607 normalization to TOC, have generated a Hg/TOC spike. At Meghalaya, Bottaccione and Højerup, one
608 Hg/TOC spike is observed below the KPg boundary, within the age interval of the planktic
609 foraminiferal CF2 biozone (labeled I; Figs. 8A, B and 10A). This spike in the Bot- taccione section is
610 located about 4 m below the KPg boundary and is somewhat smaller than in the Meghalaya section. At
611 Padriciano, a large Hg/TOC spike is observed below the KPg boundary and, perhaps, can be correlated
612 with the spike described above, but presence of planktic foraminifers typical of the CF2eCF1 biozones
613 has not been observed and, therefore, do not support such a correlation (Fig. 8C).
614 A second Hg/TOC spike is present at the KPg boundary at Højerup, Bottaccione, and Meghalaya
615 (labeled II in Figs. 8A, B and 10A). Similar to the Hg/TOC spike I, the size of spike II is variable from
616 place to place, being larger at Højerup. At the Padriciano section (Fig. 8C), this spike is absent as the
617 KPg boundary is marked by an unconformity. Two large Hg/TOC spikes are present in the Jhilmili
618 section within the planktic foraminiferal subzone P1a (labeled III and IV; Fig. 10B). At Højerup, a
619 Hg/TOC spike is seen about 1e1.5 m above the KPg boundary (labeled III, Fig. 8A), about 4 m above
620 the KPg boundary at Bottaccione and about 0.5 m above at Meghalaya.
621 At the Bajada del Jagüel section, a large Hg/TOC spike is observed in the sandstone layer that marks
622 the unconformity at the KPg boundary (Fig. 9). The presence of volcanoclastic sedimentary grains in
623 the sandstone is an evidence of local volcanism adjacent to the Neuqueñ Basin that may have
624 contributed to enhancing the Hg/ TOC ratio background prior to the KPg boundary. This positive Hg/
625 TOC excursion may correspond to the Hg/TOC enrichment (spike II) recorded in the Højerup and
626 Bottaccione sections. However, the paucity of the record of the CF1, Po, Pa and P1a planktic forami-

627 niferal biozone interval, as pointed out by Keller et al. (2007), attest to a depositional or erosional
628 hiatus of about 700 kyr bracketing the KPg boundary. Therefore, this Hg enrichment is possibly related
629 to local volcanism next to this basin and the absence of spikes I and III could be justified by this
630 depositional/erosional hiatus.
631 Covariation between Hg and Al_2O_3 (mostly associated with clays) is observed in some sections across
632 the KPg boundary and this led to the suggestion that Hg was probably adsorbed onto continental clays
633 with subsequent transport and deposition into the sea (e.g. Sial et al., 2013). However, there is no clear
634 correlation between Al_2O_3 and Hg/TOC (Tables 1-3), except in the KPg boundary layer at Højerup
635 (Fiskeler Member).
636 Molybdenum in sedimentary rocks has been suggested as an important elemental proxy for anoxia (e.g.
637 Bond et al., 2015; Grasby et al., 2015a). Based on results from the Cariaco Basin, north central coast of
638 Venezuela, Lyons et al. (2003) demonstrated a high cor- relation between TOC content and Mo/Al
639 ratio in euxinic sediments and, therefore, Mo/Al trends may allow calculating the TOC composition.
640 According to Wilde et al. (2004), however, this method demands refinement and no universal
641 elemental proxy for determining TOC has been established so far. Mo/Al ratios are useful for
642 discerning the original compositions of ancient rocks that were subjected to later diagenetic, low-grade
643 metamorphism or weathering.
644 Molybdenum concentrations, analyzed in almost all samples in this study, have been normalized to
645 corresponding Al values (Figs. 8Ae10B). At Højerup, low values of Mo/Al ratio characterize the
646 topmost Maastrichtian (0.50 cm below the KPg boundary) and no correlation is observed between this
647 ratio and TOC. Within the Fiskeler Member clays, Mo/Al ratios are enhanced, while $\delta^{13}C$ org changes
648 to higher values and a positive shift of TOC values is observed. In the Cerithium Limestone and Stevns
649 Klint Formation, in the lower Danian, no correlation between TOC and Mo/Al is apparent and Mo/Al
650 ratios are higher than in the Fiskeler Member.

At Bottaccione, Mo/Al ratios are low, with a monotonous strat- igraphic variation curve in the upper Maastrichtian, but a negative shift is seen about 0.50 cm below the KPg boundary, coinciding with vigorous positive-negative shifts in TOC values followed by a positive one of Mo/Al at the KPg boundary. At Meghalaya, Mo/Al ratios are low in the upper Maastrichtian, but likewise Højerup and Bottaccione, it shifts to lower values within 20 cm below the KPg boundary, opposite to TOC values which exhibit higher values. In the Bajada del Jagüel section, Mo/Al ratios are also low, but with little variation and no particular correlation with TOC is apparent. In the Danian Jhilmili section, Mo/Al ratios are low, and in the lower half of this section no correlation is seen with TOC but in the upper half of the section there is a weak correlation with TOC values. In the Bottaccione, Padriciano, Meghalaya, and Bajada del Jagüel sec- tions, minimum Mo/Al ratios do not coincide with $\delta^{13}C$ org peaks. The Højerup section is the only one which departs from this rule.

Lowrie et al. (1990) investigated the origin of the whitish limestone beds at about 20e50 cm below the KPg boundary in the Bottaccione and Contessa sections at Gubbio. They believed that these white beds were deposited under the same conditions as the underlying pink beds of the Scaglia Rosa Formation whose whit- ening is related to removal of Fe2þ ions by downward infiltration of reducing waters resulting from large quantity of organic matter produced by the extinction at the KPg boundary. However, Abrajevitch et al. (2015) demonstrated that a process of downward percolation of organic-rich fluids is unlikely at Bidart and Gubbio and the stratigraphic record of Mo/Al redox proxy in the studied KPg sections here suggests that Hg/TOC spikes are likely not related to decrease in oxygenation. Therefore, anoxia was not the main cause for anomalous Hg/TOC observed across the KPg boundary.

6.3. Hg isotopes

Mercury isotope analyses for the Hg spikes in the complete Højerup (Fiskeler Member), Bottaccione (Scaglia Rossa Formation) and Meghalaya sections, besides Jhilmili, Padriciano and Bajada del Jagüel sections are listed in Table 4, with results reported in delta notation in permil (‰) relative to NIST SRM 3133 Hg standard. Six analyses from a section at Bidart, part of the Basque basin, France, one of the most complete KPg boundary successions known (Bonté et al., 1984; Galbrun and Gardin, 2004; Font et al., 2014, 2016), were included for comparison and are plotted alongside the analyses for all sections in this study in Fig. 11. In this Figure, δ^{202}Hg (MDF) for all analyzed samples were plotted against corresponding Δ^{201}Hg (MIF) values and the ranges for volcanic emission and chondrite/volcanic emission Hg are indicated.

Two samples from the Meghalaya section yielded δ^{202}Hg values of -1.61‰ (spike I) and -1.89‰ (spike II) and Δ^{201}Hg close to 0.0‰. Three among four of the analyzed samples (spike II) from the Fiskeler Member at Højerup yielded δ^{202}Hg between -1.00 and -2.00‰ and two of them display positive Δ^{201}Hg or negative but very close to 0.0‰. One sample from the KPg boundary layer at the Bottaccione section in Gubbio (Spike II) yielded a δ^{202}Hg value of -1.28‰ and positive Δ^{201}Hg. In addition, Hg isotopes were analyzed in six samples from Bidart which yielded δ^{202}Hg values from -0.25 to -2.66 and all positive Δ^{201}Hg values (Fig. 11). A sample from the KPg boundary layer from which Font et al. (2016) determined a true Hg spike (corresponding to spike II in this study) yielded a δ^{202}Hg value of -0.74 compatible with volcanic or chondrite source Hg. So, in the light of or current Hg isotope data, a volcanic source for Hg in the KPg boundary (spike II) is likely at these classical KPg localities.

One sample from the Padriciano locality (spike I) yielded a δ^{202}Hg value of -1.38‰ and slightly positive Δ^{201}Hg, and as in Meghalaya, Hg isotopes seem to support volcanic source for the spike I in these two localities. One sample from spike III at the Jhilmili site showed a value of -1.01‰ and negative Δ^{201}Hg while another sample (spike labeled IV) yielded a δ^{202}Hg value of -2.18‰ and a Δ^{201}Hg value of -0.28‰. While the Hg isotope signature for spike III seems to support a volcanic

698 origin, the one for spike IV suggests some post-depositional alteration. Among the twelve samples
699 from Jagüel Formation, nine show δ^{202}Hg between -1.00 and -2.00‰ and Δ^{201}Hg are all positive,
700 compatible with a volcanic source Hg.
701 Interestingly, most of the analyzed samples in this study show slightly, but significantly higher than the
702 analytical precision of 0.04‰, positive Δ^{201}Hg signatures. Since most continental samples (soils,
703 sediments and land plants) usually display negative or close to zero Δ^{201}Hg and post-deposition and
704 diagenetic processes likely would not induce odd-MIF, the positive Δ^{201}Hg values observed in most
705 samples here indicate a long-term atmospheric transport prior to deposition. During transportation in
706 the atmosphere, photoreduction of gaseous oxidized Hg (GOM) would enrich odd isotopes in water
707 droplets and particles, for example by adsorption, thus triggering positive Δ^{201}Hg values in final
708 deposition (Chen et al., 2012; Blum et al., 2014). Our results seem point to Hg iso- topes as a
709 promising way for identification of the Hg source.
710
711 7. Discussion
712 From the Hg/TOC stratigraphic patterns in this study, one is tempted to outline a preliminary picture of
713 the global Hg loading to the environment during the 750 kyr of Deccan phase-2 volcanic eruptions.
714 However, as organic matter content in the examined sections tend to be very low (<0.2%), reliable
715 Hg/TOC ratios are not always obtained and so these ratios should be looked with caution.
716 Three Hg/TOC spikes are depicted from the three examined complete sections. One of them observed
717 within the CF2 foraminiferal biozone in Meghalaya, Højerup and Bottaccione sections (spike-I), in
718 agreement with increased Hg loading to the atmosphere by early stages of Deccan phase-2 eruptions,
719 between 250 and 160 Kyr before the KPg boundary. Too low TOC values at Højerup and Bottaccione
720 resulted at enrichment of the Hg spike I in these two sections. As there is no foraminifer biozone
721 control at Padriciano, we speculate that the prominent Hg enrichment observed at this section (182

722 ng.g^{-1}of Hg), about one meter below the KPg boundary, is coeval with the spike-I in the Meghalaya
723 section. An apparent Hg spike (16 ng.g^{-1}) at about one meter below the KPg boundary at Bajada del
724 Jagüel, recognized by Sial et al. (2014), disappears after TOC normalization.
725 It became evident from this study that a second Hg/TOC spike (spike-II) coincides with the KPg
726 boundary layer at Højerup and Bottaccione. At Meghalaya, presence of an Hg enhancement in the
727 proximity of the KPg boundary becomes evident only after normalization of the Hg concentration to
728 TOC. In this case, a proximal section to the Deccan, the Hg loading was only detected after
729 normalization to TOC. Enrichment of Hg in the KPg boundary at Padriciano, if any, was probably
730 swept off by erosion that pre- ceded deposition of the breccia that marks this boundary. It is uncertain
731 whether the notable Hg/TOC spike in the KPg boundary at Bajada del Jagüel is correlated to spike II or
732 resulted from Hg loading from local volcanism within the Neuqueñ Basin. A third Hg/ TOC spike in
733 the Danian (spike III) at Jhilmili, a very proximal sec- tion at the Deccan volcanic center, Højerup,
734 Bottaccione and Meghalaya within the P1a foraminiferal biozone, seems to be a record of late stages of
735 Deccan phase-2 eruptions within the 220-500 kyr after the KPg boundary.
736 Around 66 Ma ago, the Højerup and Bottaccione sites were located at similar distances relative to both
737 the Deccan Traps and the Chicxulub impact site (Fig. 1), therefore similar-sized Hg peaks would be
738 expected. “Two explanations for the observed discrepancy may be offered: (a) divergence in time
739 lengths and/or factors governing Hg deposition, (b) preservation of Hg deposit from weathering and
740 diagenesis. The high level of Hg recorded at the KPg boundary layer at Højerup may have resulted
741 from an increased flux of volcanic-derived Hg from the landmass into the marine realm. At
742 Bottaccione, Hg accumulation likely resulted from a similar mechanism, but a distal, deep marine
743 (pelagic) setting probably determined a lower Hg concentration if compared to the more proximal
744 Højerup section. However, as the KPg boundary layer has been tectonically tilted at Bottaccione, this
745 could have also facilitated a gradual Hg leaching, resulting in a more modest remaining Hg

746 enrichment" (Sial et al., 2014, p. 111e112). One cannot discard the possibility of acid rain leaching of
747 Hg in the aftermath of the KPg boundary event. It is difficult to estimate how much mountain chains,
748 dispersion corridors along latitudinal zones, winds and marine currents have affected the Hg transport
749 and deposition during the KPg transition. Due to climate changes, the environment at that time was
750 probably depleted of organic scav- enging capacity and, therefore, Hg^{+2} was likely kept in solution,
751 readily adsorbed onto clays and transported to the sea/ocean.
752 Large differences in Hg peak magnitude, as observed between Højerup and Bottaccione, are also
753 observed in sections bracketing the KPg boundary within a single basin (e.g. Salta and Neuqueñ basins;
754 Sial et al., 2013, 2014). One cannot totally discard the pos- sibility that the Chicxulub asteroid impactor
755 may have carried a large amount of Hg. If Hg concentrations measured in the CI- chondrite Orgueil
756 were typical for the KPg boundary asteroid impactor, full release of highly volatile Hg would
757 correspond to a total injected mass of 10^6-10^7 metric tons of Hg according to Meier et al. (2015), that
758 is, 10^4-10^5 times higher than present annual anthropogenic emissions, implying a global Hg deposit of
759 several thousand ng Hg/cm^2. Small Hg peaks recorded at the KPg boundary have been attributed to
760 terrestrial response to the Chicxulub impact by Hildebrand and Boynton (1989) or to volcanic activity
761 pulses (Sial et al., 2013, 2014; Font et al., 2016). Meier et al. (2015) measured the concentration and
762 isotopic composition of Hg in meteorites and at some KPg boundary sites, including Højerup, Bidart
763 (France) and Teapot Dome sites (USA). At Teapot Dome, they found a huge, double-spiked Hg peak of
764 ~1000 $ng.g^{-1}$, and much smaller Hg concentrations at Højerup (200 $ng.g^{-1}$) and Bidart (80 $ng.g^{-1}$). The
765 Hg isotopic composition in Hg spikes in sedi- mentary rocks spanning the KPg boundary can
766 potentially help constraining the Hg source. Meier et al. (2015) did not report Hg isotope compositions
767 measured in their study of meteorites and KPg boundary sites to allow further comparison with the Hg
768 isotope data reported in the present study.

769 The $\delta^{202}Hg$ data in clays from the KPg boundary layer at Højerup, from the KPg boundary clay layer in
770 the Scaglia Rossa Formation at Bottaccione and from Meghalaya (spike II) besides from Hg in the
771 spike I (Meghalaya and Padriciano) and spike III at Jhilmili lie within the range for volcanogenic Hg
772 (0.00 to -2.00‰) as reported by Bergquist and Blum (2009). The small and positive $\Delta^{201}Hg$ (Table 4)
773 also sheds light on the long-range atmospheric transport of volcanic emission.
774
775 8. Conclusions
776 (a) Three Hg/TOC spikes present in the studied complete sections (Meghalaya, Højerup and
777 Bottaccione) are proposed to represent a record of the Deccan phase-2 eruptions. One of these spikes is
778 situated within the CF2 foraminiferal biozone (e.g. Meghalaya), within the 250 kyr (beginning of
779 Deccan phase-2) and 160 kyr (CF2-CF1biozones boundary) before the KPg boundary after carbon
780 dioxide, sulfuric aerosols and other toxic agents reached a critical threshold. The second spike, at the
781 KPg boundary, is also coeval to the Deccan phase-2 (e.g. Højerup and Bottaccione) and a third one,
782 within the P1a foraminiferal biozone in the lowermost Danian (e.g. Jhilmili), is likely related to late
783 Deccan phase-2 eruptions (within the 220-500 kyr interval after the KPg boundary). These three
784 periods of anomalous Hg deposition identified here suggest events of enhanced Hg deposition over
785 broad areas of the globe.
786 b) The possibility that Hg enhancements around the KPg boundary at Højerup, Bottaccione, and
787 Meghalaya, could be postdepostional, resulting from scavenging by anoxia on the seafloor and
788 transported downward into the uppermost 50 cm layer, is not confirmed by the stratigraphic record of
789 Mo/Al redox proxy that does not support a decrease in oxygenation.
790 (c) Differences in the magnitude of the Hg concentrations among the complete studied sections are due
791 to either dif- ference in sedimentation rates, proximity to the continents, or to the partial leaching of Hg
792 during weathering and/or diagenesis.

(d) In selecting Hg enriched values that may represent true volcanic Hg loading to the environment, it is a common practice to normalize Hg concentrations by the corresponding TOC % values. This approach potentially confirms true Hg enrichments but inaccuracy of measurements may lead to highly variable or unrealistic Hg/TOC spikes in cases where extremely low TOC values (<0.2%) are used (e.g. uppermost Danian portion of the Meghalaya section).

(e) The δ^{202}Hg data for boundary clays or from samples of other sedimentary rocks spanning the KPg boundary lie within the range of volcanogenic Hg. Small and positive Δ^{201}Hg seems to support a long range atmospheric transport of Hg. This indicates a promising start of using Hg isotopes in the identification of the Hg source.

Despite these stimulating results, one cannot assure that Hg is volcanogenic solely based on isotopic similarity because of: (a) limited amount of Hg isotope data, and (b) processes involved as eruption, transportation and even deposition may have lead to Hg isotope fractionation/modification of the original Hg isotope signals.

We hope this study contributes to the growing agreement that a single large asteroid/comet impact could not have been the sole cause of the end-Cretaceous mass extinction, but rather a contributing factor along with volcanism.

Acknowledgments

We thank Gilsa M. Santana and Vilma S. Bezerra for assistance with stable isotope analyses in the LABISE and to Ingra K.C. Belmino for the help with the Hg analyses at the LABOMAR. We acknowledge N. Thibault (Copenhagen) for discussions about stratigraphic details of Danish successions. We are grateful to Prof. Finn Surlyk (University of Copenhagen) and to an anonymous reviewer whose comments and suggestions on an earlier version of the manuscript greatly contributed to improve it. MKP and VCT are grateful to the Brazilian Council for Scientific and Technological Development (CNPq) for three-month visiting professor fellowships in the LABISE, Brazil. V.C. Tewari is thankful

817 to Dr. A.K. Gupta, Director of WIHG, for collaborative project between this Institution and the
818 NEGeLABISE. Samples from Bidart (6) analyzed for Hg isotopes in this study were provided by Eric
819 Font to whom we are grateful. This study was partially supported by grants from National “973”
820 (2013CB430001), Strategic Priority Research Program of CAS (n. XDB05030302) and NSF China
821 (41273023) to JBC, and to ANS (CNPq grants n. 472842/2010-2 and 471013/2012-9 and FACEPE
822 grants APQ 0727-1.07/08 and APQ-1059-9.05/12) and CNPq grant no. 576.601/2009-1 to LDL.
823 Financial support through the Danish Agency for Science, Technology and Innovation (grant n. 11-
824 103378) to RF and through the Danish National Research Founda- tion's Center of excellence
825 NordCEE (DNRF grant n. DNRF53) is highly appreciated. This is the NEGeLABISE contribution n.
826 272.

827

828 References

829 Aberhan, M., Weidemeyer, S., Kiessling, W., Scasso, R.A., Medina, F.A., 2007. Faunal evidence for
830 reduced productivity and uncoordinated recovery in Southern Hemisphere CretaceousPaleogene
831 boundary sections. Geology 35, 227-230.
832 Abrajevitch, A., Font, E., Florindo, F., Roberts, A.P., 2015. Asteroid impact vs. Deccan eruptions: the
833 origin of low magnetic susceptibility beds below the Cretaceous- Paleogene boundary revisited.
834 Earth Planetary Science Letters 430, 209-223.
835 Aguirre-Urreta, B., Tunik, M., Naipauer, M., Pazos, P., Ottone, E., Fanning, M., Ramos, V.A., 2011.
836 Malargüe group (MaastrichtianeDanian) deposits in the Neuquén
837 Andes,Argentina:implicationsfortheonsetofthefirstAtlantic transgression related to Western
838 Gondwana break-up. Gondwana Research 19, 482-494.
839 Alvarez, W., 2009. The historical record in the Scaglia limestone at Gubbio: mag- netic reversals and
840 the CretaceouseTertiary mass extinction. Sedimentology 56, 137-148.

841 Alvarez, L.W., Alvarez, W., Asaro, F., Michel, H.V., 1980. Extraterrestrial cause for the
842 CretaceouseTertiary extinction. Science 208, 1095-1108.
843 Banerji, R.K., 1981. CretaceouseEocene sedimentation, tectonism and biofacies in the Bengal Basin,
844 India. Palaeogeography, Palaeoclimatology, Palaeoecology 34, 57-85.
845 Berggren, W.A., Kent, D.V., Swisher III, C.C., Aubry, M.P., 1995. A revised Cenozoic geochronology
846 and chronostratigraphy. In: Berggren, W.A., Kent, D.V., Aubry, M.-P., Hardenbol, J. (Eds.),
847 Geochronology, Time Scales and Stratigraphic Correlation, Society of Economic Paleontologists
848 and Mineralogists, Special Volume No. 54, pp. 129-212.
849 Bergquist, B.A., Blum, J.D., 2009. The odds and evens of mercury isotopes: appli- cations of mass-
850 dependent and mass-independent isotope fractionation. Ele- ments 5, 353-357.
851 Bertels, A., 1975. Bioestratigrafía del Paleogeno en la República Argentina. Revista Espan~ola de
852 Micropaleontologia 8, 429-450.
853 Bhandari, N., Shukla, P.N., Cini Castognoli, G., 1993. Geochemistry of some K/T sections in India.
854 Palaeogeography, Palaeoclimatology, Palaeoecology 104, 199-211.
855 Bhandari, N., Gupta, M., Panday, J., Shukla, P.N., 1994. Chemical profiles in K/T boundary section of
856 Meghalaya, India: cometary, asteroidal or volcanic. Chemical Geology 113, 45-60.
857 Blum, J.D., Sherman, L.S., Johnson, M.W., 2014. Mercury isotopes in earth and environmental
858 sciences. Annual Reviews of Earth Planetary Science 42, 249-269.
859 Bond, D.P.G., Wignall, P.B., 2014. Large igneous provinces and mass extinctions: an update.
860 Geological Society of America Special Paper 505 29e55.
861 Bond, D.P.G., Wignall, P.B., Joachimski, M., Sun, Y., Savov, I., Grasby, S.E., Beauchamp, B.,
862 Blomeier, D.P.G., 2015. An abrupt extinction in the Middle Permian (Capitanian) of the Boreal
863 Realm (Spitsbergen). Geological Society of America Bulletin. http://dx.doi.org/10.1130/B31216.1.

Bonte , P., Delacotte, O., Renard, M., Laj, C., Boclet, D., Jehanno, C., Rocchia, R., 1984. An iridium rich layer at the Cretaceous Tertiary boundary in the Bidart Section (Southern France). Geophysical Research Letters 11, 473e476.

Caffau, M., Plenicar, M., Pugliese, N., Drobne, K., 1998. Late Maastrichtian rudists and microfossils in the Karst region (NE Italy and Slovenia). Geobios, Memoire Special 22, 37-46.

Callegaro, S., Baker, D.R., De Min, A., Marzoli1, A., Geraki, K., Bertrand, H., Viti, C., Nestola, F., 2014. Microanalyses link sulfur from large igneous provinces and Mesozoic mass extinctions. Geology 42, 895e-898.

Casadío, S., 1998. Las ostras del límite CretacicoePaleogeno de la cuenca Neuquina (Argentina). Su importancia bioestratigrafica y paleobiogeografica. Ame- ghiniana 35, 449e-471.

Chen, J.-B., Hintelmann, H., Dimock, B., 2010. Chromatographic pre-concentration of Hg from dilute aqueous solutions for isotopic measurement by MC-ICP-MS. Journal of Analytical Atomic Spectrometry 25, 1402-1409.

Chen, J.-B., Hintelmann, H., Feng, X.-B., Dimock, B., 2012. Unusual fractionation of both odd and even mercury isotopes in precipitation from Peterborough, ON, Canada. Geochimica et Cosmochimica Acta 90, 33-46.

Chenet, A.L., Courtillot, V., Fluteau, F., Gerard, M., Quidelleur, X., Khadri, S.F.R., Subbarao, K.V., Thordarson, T., 2009. Determination of rapid Deccan eruptions across the CretaceouseTertiary boundary using paleomagnetic secular variation: 2. Constraints from analysis of eight new sections and synthesis for a 3500-m-thick composite section. Journal of Geophysical Research 114, 1-38.

Coccioni, R., Premoli Silva, I., 2015. Revised Upper AlbianeMaastrichtian planktonic foraminiferal biostratigraphy and magneto-stratigraphy of the classical Tethyan Gubbio section (Italy). Newsletters on Stratigraphy 48, 4790.

887 Coccioni, R., Frontalini, F., Bancalà, G., Fornaciari, E., 2010. The Dan-C2 hyperthermal event at
888 Gubbio (Italy): global implications, environmental effects, and cause(s). Earth and Planetary
889 Science Letters 297 (2010), 298-305.
890 Cripps, J.A., 2002. Environmental Impact of Deccan Trap Flood Basalt Volcanism: Assessment of
891 Regional Floral Responses to Late Cretaceouseearly Tertiary Activity. Ph.D. Thesis, Open
892 University, Milton Keynes, UK, 502 pp.
893 Drobne, K., Ogorelec, B., Plenicar, M., Barattolo, F., Turnsek, D., Zucchi Stolfa, M.L., 1989. The
894 Dolenja Vas section, a transition from Cretaceous to Palaeocene in the NW Dinarides, Yugoslavia.
895 Memorie e Societa Geologica Italiana 40, 73-84.
896 Estrade, N., Carignan, J., Donard, O.F.X., 2011. Tracing and quantifying anthropogenic mercury
897 sources in soils of northern France using isotopic signatures. Envi- ronmental Science and
898 Technology 45, 1235-1242.
899 Font, E., Fabre, F., Nédélec, A., Adatte, T., Keller, G., Veiga-Pires, C., Ponte, J., Mir~ao, Jose ,
900 Khozyem, H., Spangenberg, J., 2014. Atmospheric halogen and acid rains during the main phase of
901 Deccan eruptions: magnetic and mineral evi- dence. Geological Society of America Special paper
902 505 1-16.
903 Font, E., Adatte, T., Sial, A.N., Lacerda, L.D., Keller, G., Punekar, J., 2016. Mercury anomaly, Deccan
904 volcanism and the end-Cretaceous mass extinction. Geology 44, 171-174.
905 Foucher, D., Ogrinc, N., Hintelmann, H., 2009. Tracing mercury contamination from the Idrija mining
906 region (Slovenia) to the Gulf of Trieste using Hg isotope ratio measurements. Environmental
907 Science & Technology 43, 33-39.
908 Galbrun, B., Gardin, S., 2004. New chronostratigraphy of the Cretaceous-Paleogene boundary interval
909 at Bidart (France). Earth and Planetary Science Letters 224, 19-32.

910 Galeotti, S., Moretti, M., Cappelli, C., Phillips, J., Lanci, L., Littler, K., Monechi, S., Petrizzo, M.R.,
911 Premoli Silva, I., Zachos, J.C., 2015. The Bottaccione section at Gubbio, central Italy: a classical
912 Paleocene Tethyan setting revisited. Newslet- ters on Stratigraphy 48, 325-339.
913 Garg, R., Khowaja-Ateequzzaman, Prasad, V., 2006. Significant dinoflagellate cyst Biohorizons in the
914 Upper CretaceousePalaeocene succession of the Khasi Hills, Meghalaya. Journal Geological Society
915 India 67, 737-747.
916 Gehrke, G.E., Blum, J.D., Marvin-DiPasquale, M., 2011. Sources of mercury to San Francisco Bay
917 surface sediment as revealed by mercury stable isotopes. Geo- chimica et Cosmochimica Acta 75,
918 691-705.
919 Gertsch, B., Keller, G., Adatte, T., Garg, R., Prasad, V., Berner, Z., Fleitmann, D.S., 2011.
920 Environmental effects of Deccan volcanism across the CretaceouseTertiary transition in Meghalaya,
921 India. Earth and Planetary Science Letters 310, 272-285.
922 Grasby, S.E., Sanei, H., Beauchamp, B., Chen, Z., 2013. Mercury deposition through the
923 PermoeTriassic Biotic Crisis. Chemical Geology 351, 209-216.
924 Grasby, S.E., Beauchamp, B., Bond, D.P.G., Wignall, P.B., Sanei, 2015a. Mercury anomalies
925 associated with three extinction events (Capitanian Crisis, Latest Permian Extinction and the
926 Smithian/Spathian Extinction) in NW Pangea. Geological Magazine.
927 http://dx.doi.org/10.1017/S0016756815000436.
928 Grasby, S.E., Beauchamp, B., Bond, D.P.G., Wignal, P., Talavera, C., Galloway, J.M., Piepjohn, K.,
929 Reinhardt, L., Blomeier, D., 2015b. Progressive environmental deterioration in northwestern Pangea
930 leading to the latest Permian extinction. Geological Society of America Bulletin 127, 1311-1347.
931 Gregoric, M., Caffau, M., Lenaz, D., De Min, A., 1998. Late MaastrichitianePalaeocene unaltered
932 glassy microspherules at Padriciano, Trieste Karst, NE Italy: a pre- liminary report. Razprave 4,
933 Razreda SAZU 211e233.

934 Grotzinger, J.P., Fike, D.A., Fischer, W.W., 2011. Enigmatic origin of the largest known carbon
935 isotope excursion in Earth's history. Nature Geosciences 4, 285-292.
936 Habib, D., Saeedi, F., 2007. The Manumiella seelandica global spike: cooling during regression at the
937 close of the Maastrichtian. Palaeogeography, Palae- oclimatology, Palaeoecology 255, 87-97.
938 Hansen, T., Surlyk, F., 2014. Marine macrofossil communities in the uppermost Maastrichtian chalk of
939 Stevns Klint, Denmark. Palaeogeography, Palae- oclimatology, Palaeoecology 399, 323-344.
940 Hansen, H.J., Toft, P., 1996. Dolenja Vas and its carbon isotopes. In: Drobne, K., Gorican, S.., Kotnik,
941 B. (Eds.), Int. Workshop Postojna'96. The Role of Impact Processes in the Geological and
942 Biological Evolution of Planet Earth, pp. 31-32.
943 Hansen, H.J., Drobne, K., Gwozda, R., 1995. The K/T boundary in Slovenia: dating by magnetic
944 susceptibility stratigraphy and an iridium anomaly in a debris flow. In: Montanari, A., Coccioni, R.
945 (Eds.), 4th International Workshop ESF Sci. Network “Impact Cratering and Evolution of Planet
946 Earth”, Ancona. The Role of Impacts on the Evolution of the Atmosphere and Biosphere with
947 Regard to Shortand Long-Term Changes. Abstract and Field Trips, pp. 81-82.
948 Hart, M.B., Feist, S.E., Price, G.D., Leng, M.J., 2004. Reappraisal of the KeT boundary succession at
949 Stevns Klint, Denmark. Journal of the Geological Society of London 161, 1-8.
950 Heredía, S., Salgado, L., 1999. Posicio n estratigra fica de los estratos supracretacicos portadores de
951 dinosaurios en Lago Pellegrini, Patagonia Septentrional, Argentina. Ameghiniana 36, 229-234.
952 Hildebrand, A.R., Boynton, W.V., 1989. Hg anomalies at the K/T boundary: evidence for acid rain?
953 Meteoritics 24, 277-278.
954 Howell, J.A., Schwarz, E., Spalletti, L.A., Veiga, G.D., 2005. The Neuque n Basin: an overview. In:
955 Veiga, G.D., Spalletti, L.A., Howell, J.A., Schwarz, E. (Eds.), The Neuque n Basin, Argentina: A
956 Case Study in Sequence Stratigraphy and Basin Dynamics, Geological Society, London, Special
957 Publications, 252, pp. 1-14.

958 Hsü, K.J., McKenzie, J.A., 1985. A “Strangelove” ocean in earliest Tertiary. In: Sundquist, E.T.,
959 Broecker, W.S. (Eds.), Carbon Cycle and Atmosphere CO2 Natural Variations Archean to Present.
960 Washington, D.C., American Geophysical Union, Geophysical Monograph, 32, pp. 487-492.
961 Huang, Q., Liu, Y.-L., Chen, J.-B., Feng, X.-B., Huang, W.-L., Yuan, S.-L., Cai, H.-M., Fu, X.-W.,
962 2015. An improved dual-stage protocol to pre-concentrate mercury from airborne particles for
963 precise isotopic measurement. Journal of Analytical Atomic Spectrometry 30, 957-966.
964 Jiskra, M., Wiederhold, J.G., Bourdon, B., Kretzschmar, R., 2012. Solution and speciation controls of
965 mercury isotope fractionation of Hg(II) sorption to goethite. Environmental Science and Technology
966 46, 6654-6662.
967 Jourdan, F., Hodges, K., Sell, B., Schaltegger, U., Wingate, M.T.D., Evins, L.Z., Soderlund, U.,
968 Haines, P.W., Phillips, D., Blenkinsop, T., 2014. High-precision dating of the Kalkarindji large
969 igneous province, Australia, and synchrony with the EarlyeMiddle Cambrian (Stage 4e5) extinction.
970 Geology 42, 543-546.
971 Keller, G., Kerr, A.C., 2014. Foreword. In: Keller, G., Kerr, A.C. (Eds.), Volcanism, Impacts, and
972 Mass Extinctions: Causes and Effects, Geological Society of America Special Paper, 505, pp. veix.
973 Keller, G., Adatte, T., Tantawy, A.A., Berner, Z., Stinnesbeck, W., Stueben, D., Leanza, H.A., 2007.
974 High stress late Maastrichtian and early Danian palaeoenvironment in the Neuqueñ Basin,
975 Argentina. Cretaceous Research 28, 939-960.
976 Keller, G., Adatte, T., Gardin, S., Bartolini, A., Bajpai, S., 2008. Main Deccan volcanism phase ends
977 near the KeT boundary: evidence from the KrishnaeGodavari Ba- sin, SE India. Earth Planetary
978 Science Letters 268, 293-311.
979 Keller, G., Khosla, S.C., Sharma, R., Khosla, A., Bajpai, S., Adatte, T., 2009. Early Danian Planktic
980 foraminifera from intertrappean beds at Jhilmili, Chhindwara District, Madhya Pradesh, India.
981 Journal of Foraminifer Research 39, 40e-55.

982 Keller, G., Bhowmick, P.K., Upadhyay, H., Dave, A., Reddy, A.N., Jaiprakash, B.C., Adatte, T., 2011.
983 Deccan volcanism linked to the Cretaceous-Tertiary boundary mass extinction: new evidence from
984 ONGC wells in the Krishna-Godavari Basin. Journal of the Geological Society of India 78, 399-428.
985 Keller, G., Adatte, T., Bhowmick, P.K., Upadhyay, H., Dave, A., Reddy, A.N., Jaiprakash, B.C., 2012.
986 Nature and timing of extinctions in CretaceouseTer- tiary planktic foraminifera preserved in Deccan
987 intertrappean sediments of the Krishna-Godavari Basin, India. Earth Planetary Science Letters 341,
988 211-221.
989 Keller, G., Punekar, J., Mateo, P., 2016. Upheavals during the Late Maastrichtian: volcanism, climate
990 and faunal events preceding the end-Cretaceous mass extinction. Palaeogeography,
991 Palaeoclimatology, Palaeoecology 441, 137-151.
992 Knoll, A.H., Hayes, J.M., Kaufman, A.J., Swett, K., Lambert, I.B., 1986. Secular variation in carbon
993 isotope ratios from upper Proterozoic successions of Svalbard and East Greenland. Nature 321, 832-
994 838.
995 Korte, C., Kozur, H.W., 2010. Carbon-isotope stratigraphy across the Permiane- Triassic boundary: a
996 review. Journal of Asian Earth Sciences 39, 215e235. Krishnan, M.S., 1968. Geology of India and
997 Burma. In: Krishnan, M.S. (Ed.), Madras, 536 pp.
998 Krupp, R., 1988. Physicochemical Aspects of Mercury Metallogenesis. Chemical Geology 69, 345-
999 356.
1000 Laffont, L., Sonke, J.E., Maurice, L., Hintelmann, H., Sanchez-Baccarez, Y., Perez, T.,
1001 Behra, P., 2009. Anomalous mercury isotopic compositions of fish and human hair in the Bolivian
1002 Amazon. Environmental Science and Technology 43, 8985-8990.
1003 Laffont, L., Sonke, J.E., Maurice, L., Monroy, S.L., Chincheros, J., Amouroux, D., Behra, P., 2011. Hg
1004 speciation and stable isotope signatures in human hair as a tracer for dietary and occupational
1005 exposure to mercury. Environmental Sci- enceand Technology 45, 9910-9916.

1006 Lauridsen, B.W., Bjerager, M., Surlyk, F., 2012. The middle Danian Faxe Formation e new
1007 lithostratigraphic unit and a rare taphonomic window into the Danian of Denmark. Bulletin of the
1008 Geological Society of Denmark 60, 47-60.
1009 Legarreta, L., Uliana, M.A., 1999. El Jurasico y Cretacico de la Cordillera Principal y la Cuenca
1010 Neuquina. In: Caminos, R. (Ed.), Geología Argentina, Servicio Geologico Minero Argentino,
1011 Anales 29, 16, pp. 399-416.
1012 Legarreta, L., Kokogian, D.A., Boggetti, D.A., 1989. Depositional sequences of the Malargüe group
1013 (Upper CretaceouseLower Tertiary), Neuque n Basin, Argentina. Cretaceous Research 10, 337-
1014 356.
1015 Lowrie, W., Alvarez, W., Asaro, F., 1990. The origin of the white beds below the Cretaceous Tertiary
1016 boundary in the Gubbio section, Italy. Earth Planetary Sci- ence Letters 98, 303-331.
1017 Luterbacher, H.P., Premoli Silva, I., 1964. Biostratigrafia del limite CretaceoeTerziario nell'Appennino
1018 centrale. Rivista Italiana di Paleontologia e Stratigrafia 70, 67-128.
1019 Lyons, T.W., Werne, J.P., Hollander, D.J., Murray, R.W., 2003. Contrasting sulfur geochemistry and
1020 Fe/Al and Mo/Al ratios across the last oxic-to-anoxic transi- tion in the Cariaco Basin, Venezuela.
1021 Chemical Geology 195, 131-157.
1022 Maloof, A.C., Porter, S.M., Moore, J.H., Dudas, F.O., Bowring, S.A., Higgins, J.A., Fike, D.A.,
1023 Michael, Eddy, P., 2010. The earliest Cambrian record of animals and ocean geochemical change.
1024 Geological Socity of America Bulletin 122, 1731-1774.
1025 Martínez-Cortizas, A., Pontevedra-Pombal, X., García-Rodeja, E., Novoa-Munoz, J.C., Shotyk, W.,
1026 1999. Mercury in a Spanish Peat Bog: archive of climate change and atmospheric metal deposition.
1027 Science 284, 939-942.
1028 Marton, E., Drobne, K., Cimerman, F., Cosovic, V., Kosir, A., 1995. Paleomagnetism of

1029 latest Maastrichtian through Oligocene rocks in Istria (Croatia), the Karst re- gion, and S of the Sava
1030 fault (Slovenia). In: Vlahovic, I., Velic, I., Sparica, M. (Eds.), Proc.1st Croatian Geological
1031 Congress, Zagreb, 2, pp. 355-360.
1032 McLean, D.M., 1985. Deccan Traps mantle degassing in the terminal Cretaceous marine extinctions.
1033 Cretaceous Research 6, 235-259.
1034 Meier, M.M.M., Cloquet, C., Marty, B., Ferriere, L., Koeberl, C., 2015. Hg isotopes at the K-Pg
1035 boundary. Goldschmidt Conference, Prague, 16e21 August 2015, p. 1720.
1036 Meyer, K.M., Yu, M., Lehrmann, D., van de Schootbrugge, B., Payne, J.L., 2013. Con- straints on
1037 early Triassic carbon cycle dynamics from paired organic and inorganic carbon isotope records.
1038 Earth Planetary Science Letters 361, 429-435.
1039 Mukhopadhyay, S.K., 2008. Planktonic foraminiferal succession in late Cretaceous to early Paleocene
1040 strata in Meghalaya, India. Lethaia 41, 71-84.
1041 Musso, T., Concheyro, A., Pettinari, G., 2012. Clay mineralogy and calcareous nan- nofossils from
1042 Jagüel and Roca formations in the eastern sector of Pellegrini Lake, Neuque n Basin, República
1043 Argentina. Andean Geology 393, 511-540.
1044 Nagappa, Y., 1959. Foraminiferal biostratigraphy of the Cretaceous: Eocene suc- cession in the
1045 IndiaePakistaneBurma region. Micropaleontology 5, 145e192.
1046 Nañez, C., Concheyro, A., 1997. Límite CretacicoePaleogeno. In: Geología y Recursos Minerales del
1047 Departamento Anelo, Provincia de Neuquen, República Argentina. Direccion Nacional del Servicio
1048 Geologico, Anales 25 y Direccio n Provincial de Minería Boletín, 3, pp. 12-49.
1049 Nañez, C., Parras, A., Hansen, H.J., Concheyro, A., Alonso, S., Lojen, S., Pires, M., 2002. A southern,
1050 shallow marine, CretaceousePaleogene boundary: Bajada del Jagüel Basin, Argentina. GACeMAC
1051 Annual Joint Meeting, Saskatoon, Abstracts 27, 79.

1052 Nascimento-Silva, V.M., Sial, A.N., Ferreira, V.P., Neumann, V.H., Barbosa, J.A., Pimentel, M.M.,
1053 Lacerda, L.D., 2011. CretaceousePaleogene transition at the Paraíba Basin, northeastern, Brazil:
1054 carbon-Isotope and mercury subsurface stratigraphies. Journal of South American Earth Sciences
1055 32, 379-392.
1056 Nascimento-Silva, M.V., Sial, A.N., Ferreira, V.P., Barbosa, J.A., Neumann, V.H., Pimentel, M.M.,
1057 Lacerda, L.D., 2013. Carbon isotopes, rare-earth elements and mercury behavior of
1058 MaastrichtianeDanian carbonate succession of the Paraíba Basin, Northeastern Brazil. In: Bojar,
1059 A.V., Melinte-Dobrinescu, M.C., Smit, J. (Eds.), Isotopic Studies in Cretaceous Research,
1060 Geological Society, London, Special Publications, 382, pp. 85-104.
1061 Oehlert, A.M., Swart, P.K., 2014. Interpreting carbonate and organic carbon isotope covariance in the
1062 sedimentary record. Nature Communications. http:// dx.doi.org/10.1038/ncomms5672.
1063 Ogorelec, B., Dolenec, T., Cucchi, F., Giacomich, R., Drobne, K., Pugliese, N., 1995. Sedimentological
1064 and geochemical character- istics of carbonate rocks from the K/T Boundary to lower Eocene in the
1065 Karst area (NW Adriatic Platform). 1st Croatian Geological Congress, Opatija 415-421.
1066 Outridge, P.M., Sanei, H., Stern, G.A., Hamilton, P.B., Goodarzi, F., 2007. Evidence for control of
1067 mercury accumulation in sediments by variations of aquatic primary productivity in Canadian High
1068 Arctic lakes. Environmental Science & Technol- ogy 41, 5259-5265.
1069 Pal, S., Shrivastava, J.P., Mukhopadhyay, S.K., 2015. Polycyclic aromatic hydrocarbon compound
1070 excursions and K/Pg transition in the late Cretaceouseearly Palae- ogene succession of the Um
1071 Sohryngkew river section, Meghalaya. Current Science 29, 1140-1149.
1072 Palamarczuk, S., Habib, D., 2001. Dinoflagellate evidence of the Cretaceous–Paleo- gene Boundary in
1073 Argentina. Geological Society of America, Annual Meeting, Nov. 5–8.

1074 Palamarczuk, S., Habib, D., Olsson, R.K., Hemming, S., 2002. The Cretaceous– Paleogene boundary in
1075 Argentina: new evidence from dinoflagellate, forami- niferal and radiometric dating. Geological
1076 Society of America Abstracts with Program. No. 61–20.
1077 Palinkas, A.L., Drobne, K., Durn, G., Miko, S., 1996. Mercury anomaly at the Creta- ceouseTertiary
1078 boundary: Dolenja Vas, Slovenia. In: Drobne, K., Gorican, S., Kotnik, B. (Eds.), Int. Workshop
1079 Postojna '96. The Role of Impact Processes in the Geological and Biological Evolution of Planet
1080 Earth, 31-32.
1081 Pandey, J., 1990. Cretaceous/Tertiary boundary, iridium anomaly, and foraminifer breaks in the Um
1082 Sohryngkew river section, Meghalaya. Current Science 59, 570-575.
1083 Papú, O.H., Pra mparo, M.B., Nan~ez, C., Concheyro, A., 1999. Palinología y micro- paleontología
1084 de la Formacıo n Jagüel (Maastrichtiano-Daniano), perfil Opazo, cuenca Neuquina, Argentina.
1085 Simposio Paleo geno de Ame rica del Sur. Actas Servicio Geologico Minero Argentino, Anales
1086 33, 17-31.
1087 Pardo, A., Keller, G., 2008. Biotic effects of environmental catastrophes at the end of the Cretaceous
1088 and early Tertiary: Guembelitria and Heterohelix blooms. Cretaceous Research 29, 1058-1073.
1089 Percival, L.M.E., Witt, M.L.I., Mather, T.A., Hermoso, M., Jenkyns, H.C., Hesselbo, S.P., Al-Suwaidi,
1090 A.H., Storm, M.S., Xu, W., Ruhl, M., 2015. Globally enhanced mercury deposition during the end-
1091 Pliensbachian extinction and Toarcian OAE: a link to the KarooeFerrar large igneous province.
1092 Earth and Planetary Science Letters 428, 267-280.
1093 Premoli Silva, I., Sliter, W.V., 1994. Cretaceous planktonic foraminiferal bio- stratrigraphy and
1094 evolutionary trends from the Bottacioine section, Gubbio, Italy. Palaeontographica Italica 82, 1-89.
1095 Pugliese, N., Drobne, K., Barattolo, F., Caffau, M., Galvani, R., Kedves, M., Montenegro, M.E., Pirini-
1096 Radrizzani, C., Plenicar, M., Turnsek, D., 1995. Micro- and macrofossils from K/T boundary

1097 through Paleocene in the Northern Adri- atic Platform. In: Vlahovic, I., Velic, I., Sparica, M. (Eds.),
1098 Proceedings 2, 1st Croatian Geol. Congress Opatija. Inst. Geol., Zagreb, 505-513.
1099 Pugliese, N., Arbulla, D., Caffau, M., Drobne, K., 2000. Strategia di vita nel biota daniano (SBZ 1) del
1100 Carso Triestino (Italia). Accademia Nazionale de Scienze Lett. Arti di Modena. Collana di Studi 21,
1101 215-220.
1102 Punekar, A., Mateo, P., Keller, G., 2014. Effects of Deccan volcanism on paleoenvir- onment and
1103 planktic foraminifera: a global survey. Geological Society of America Special Papers 505, 91e116.
1104 Pyle, D.M., Mather, T.A., 2003. The importance of volcanic emissions for the global atmospheric
1105 mercury cycle. Atmospheric Environment 37, 5115-5124.
1106 Raja Rao, C.S., Sahasrabudhe, S.S., Deshmukh, S.S., Raman, R., 1999. Distribution, structure and
1107 petrography of the Deccan traps, India. In: Subbarao, K.V. (Ed.), Deccan Volcanic Province,
1108 Memoir d Geological Society of India, 43, pp. 401-414.
1109 Rasmussen, J.A., Heinberg, C., Hankasson, E., 2005. Planktonic foraminifers, biostratigraphy and the
1110 diachronous nature of the lowermost Danian Cerithium limestone at Stevns Klint, Denmark.
1111 Bulletin of the Geological Society Denmark 52, 113-131.
1112 Renne, P.R., Deino, A.L., Hilgen, F.J., Kuiper, D.F., Mark, D.F., Mitchell 3rd, W.S., Morgan, E.,
1113 Mundil, R., Smit, J., 2013. Time scales of critical events around the CretaceousePaleogene
1114 boundary. Science 339, 684-687.
1115 Roos-Barraclough, F., Shotyk, W., 2003. Millennial-scale records of atmospheric mercury deposition
1116 obtained from ombrotrophic and minerotrophic peatlands in the Swiss Jura Mountains.
1117 Environmental Science & Technology 37, 235-244.
1118 Roos-Barraclough, F., Martinez-Cortizas, A., García-Rodeja, E., Shotyk, W., 2002. A 14,500 year
1119 record of the accumulation of atmospheric mercury in peat: volcanic signals, anthropogenic

1120 influences and a correlation to bromine accu- mulation. Earth and Planetary Science Letters 202,
1121 435-451.
1122 Sanei, H., Grassby, S.E., Beauchamp, B., 2012. Latest Permian mercury anomalies. Geology 40, 63e-
1123 66.
1124 Sanei, H., Outridge, P.M., Stern, G.A., Macdonald, R.W., 2014. Classification of mercury-labile
1125 organic matter relationships in lake sediments. Chemical Geology 373, 87e-92.
1126 Santos, G.M., Cordeiro, R.C., Silva Filho, E.V., Turcq, B., Lacerda, L.D., Fifield, L.K., Gomes, P.R.S.,
1127 Hauscaden, P.A., Sifeddine, A., Albuquerque, A.L.S., 2001. Chro- nology of the atmospheric
1128 mercury in Lagoa da Pata Basin, Upper Rio Negro of Brazilian Amazon. Radiocarbon 43, 801-808.
1129 Scasso, R., Concheyro, A., Kiessling, W., Aberhan, M., Hecht, L., Medina, F., Tagle, R., 2005. A
1130 tsunami deposit at the Cretaceous/Paleogene boundary in the Neuquen Basin of Argentina.
1131 Cretaceous Research 26, 283-297.
1132 Schoene, B., Samperton, K.M., Eddy, M.P., Keller, G., Adatte, T., Bowring, S., Khadri, F.R., Gertsch,
1133 B., 2015. UePb geochronology of the Deccan Traps and relation to the end-Cretaceous mass
1134 extinction. Science 347, 182-184.
1135 Schroeder, W.H., Munthe, J., 1998. Atmospheric mercury e an overview. Atmo- spheric Environment
1136 32, 809-822.
1137 Schuster, P.F., Krabbenhoft, D.P., Naftz, D.L., Cecil, L.D., Olson, M.L., Dewild, J.F., Susong, D.D.,
1138 Green, J.R., Abbott, M.L., 2002. Atmospheric mercury deposition during the last 270 years: a
1139 glacial ice core record of natural and anthropogenic sources. Environmental Science & Technology
1140 36, 2303-2310.
1141 Scotese, C.R., 2013. Map Folio 16, KT Boundary (65.5 Ma, latest Maastrichtian), PALEOMAP
1142 PaleoAtlas for ArcGIS, vol. 2. Cretaceous, PALEOMAP Project, Evanston, IL.

1143 Self, S., Jay, A.E., Widdowson, M., Keszthelyi, L.P., 2008. Correlation of the Deccan and
1144 Rajahmundry Trap lavas: are these the longest and largest lava flows on Earth? Journal of
1145 Volcanology and Geothermal Research 172, 3-19.
1146 Serra-Kiel, J., Hottinger, L., Caus, E., Drobne, K., Ferrandez, C., Jauhri, A.K., Less, G., Pavlovec, R.,
1147 Pignatti, J., SAmso, J.M., Schaub, H., Sirel, E., Strougo, A., Tambareau, Y., Tospquella, J.,
1148 Zakrebskaya, E., 1998. Larger foraminiferal
1149 biostratigraphyoftheTethyanPaloeceneandEocene.Bulletin de la Societé Geologique de France 169,
1150 281-299.
1151 Sherman, L.S., Blum, J.D., Johnson, K.P., Keeler, G.J., Barres, J.A., Douglas, T.A., 2010. Mass-
1152 independent fractionation of mercury isotopes in Arctic snow driven by sunlight. Nature
1153 Geosciences 3, 173-177.
1154 Shukla, U.K., Srivastava, R., 2008. Lizard eggs from Upper Cretaceous Lameta For- mation of
1155 Jabalpur, central India, with interpretation of depositional environ- ments of the nest-bearing
1156 horizon. Cretaceous Research. http://dx.doi.org/ 10.1016/j.cretres.2008.02.003.
1157 Sial, A.N., Gaucher, C., Silva Filho, M.A., Ferreira, V.P., Pimentel, M.M., Lacerda, L.D., Silva Filho,
1158 E.V., Cezario, W., 2010. C-, Sr-isotope and Hg stratigraphies of Neoproterozoic cap carbonates of
1159 the Sergipano Belt, Northeastern Brazil. Precambrian Research 182, 351-372.
1160 Sial, A.N., Lacerda, L.D., Ferreira, V.P., Frei, R., Marquillas, R.A., Barbosa, J.A.,-Gaucher, C.,
1161 Windmo€ller, C.C., Pereira, N.S., 2013. Mercury as a proxy for vol- canic activity during extreme
1162 environmental turnover: the Cretaceous-Paleogene transition. Palaeogeography, Palaeoclimatology,
1163 Palaeoecology 387, 153-164.
1164 Sial, A.N., Chen, J.-B., Lacerda, L.D., Peralta, S., Gaucher, C., Frei, R., Cirilli, S., Ferreira, V.P.,
1165 Marquillas, R.A., Barbosa, J.A., Pereira, N.S., Belmino, I.K.C., 2014. High-resolution Hg
1166 Chemostratigraphy: a contribution to the distinction of chemical fingerprints of the Deccan

volcanism and CretaceousPaleogene boundary impact event. Palaeogeography, Palaeoclimatology, Palaeoecology 414, 98-115.

Sonke, J.E., Blum, J.D., 2013. Advances in mercury stable isotope biogeochemistry. Chemical Geology 336, 1-4.

Sonke, J.E., Schaefer, J., Chmeleff, J., Audry, S., Blanc, G., Dupre , B., 2010. Sedimentary mercury stable isotope records of atmospheric and riverine pollution from two major European heavy metal refineries. Chemical Geology 279, 90-100.

Stern, G.A., Sanei, H., Roach, P., Delaronde, J., Outridge, P.M., 2009. Historical interrelated variations of mercury and aquatic organic matter in lake sediment cores from a subarctic lake in Yukon, Canada: further evidence toward the algal-mercury scavenging hypothesis. Environmental Science & Technology 43, 7684-7690.

Sun, R., Heimbürger, L.E., Sonke, J.E., Liu, G., Amouroux, D., Berail, S., 2013. Mercury stable isotope fractionation in six utility boilers of two large coal-fired power plants. Chemical Geology 336, 103-111.

Surlyk, F., 1997. A cool-water carbonate ramp with bryozoans mounds: Late Cre- taceouseDanian of the Danish Basin. In: James, N.P., Clarke, J.D.A. (Eds.), Cool Water Carbonates, S.E.P.M. Special Publication, vol. 56, pp. 293-307.

Surlyk, F., Damholt, T., Bjerager, M., 2006. Stevns Klint, Denmark: Uppermost Maastrichtian chalk, CretaceouseTertiary boundary, and lower Danian bryo- zoans mound complex. Bulletin of the Geological Society of Denmark 54, 1-48.

Surlyk, F., Rasmussen, S.L., Boussaha, M., Schiøler, P., Schovsbo, N.H., Sheldon, E., Stemmerik, L., Thibault, N., 2013. Upper CampanianeMaastrichtian hol- ostratigraphy of the eastern Danish Basin. Cretaceous Research 46, 232-256.

1190 Svensen, H., Planke, S., Polozov, A.G., Schmidbauer, N., Corfu, F., Podladchikov, Y.Y., Jamtveit, B.,
1191 2009. Siberian gas venting and the end-Permian environmental crisis. Earth and Planetary Science
1192 Letters 277, 490-500.
1193 Tewari, V.C., Stenni, B., Pugliese, N., Drobne, K., Riccamboni, R., Dolenec, T., 2007. Peritidal
1194 sedimentary depositional facies and carbon isotope variation across K/ T boundary carbonates from
1195 NW Adriatic platform. Palaeogeography, Palae- oclimatology, Palaeoecology 255, 64-76.
1196 Tewari, V.C., Lokho, K., Kumar, K., Siddaiah, N.S., 2010a. Late CretaceousePaleocene Basin
1197 architecture and evolution of the Shillong Shelf sedimentation, Megha- laya, Northeast India.
1198 Journal of Indian Geological Congress 22, 61-73.
1199 Tewari, V.C., Kumar, K., Lokho, K., Siddaiah, N.S., 2010b. Lakadong Limestone: Paleocene-Eocene
1200 boundary carbonate sedimentation in Meghalaya, north- eastern India. Current Science 98, 88-94.
1201 Thibault, N., Harlou, R., Schovsbo, N.H., Stemmerik, L., Surlyk, F., 2015. Late Creta- ceous (Late
1202 CampanianeMaastrichtian) sea surface temperature record of the Boreal Chalk Sea. Climate of the
1203 Past Discussion 11, 5049e5071. http:// dx.doi.org/10.5194/cpd-11-5049-2015.
1204 Uliana, M.A., Biddle, K.T., 1988. MesozoiceCenozoic paleogeographic and geo- dynamic evolution of
1205 southern South America. Revista Brasileira de Geociencias 18, 172-190.
1206 Vandal, G.M., Fitzgerald, W.F., Boutron, C.F., Candelon, J.P., 1993. Variations in mercury deposition
1207 to Antarctica over the past 34,000 years. Nature 362, 621-623.
1208 Vergani, G.D., Tankard, A.J., Belotti, H.J., Welsink, H.J., 1995. Tectonic evolution and
1209 paleogeography of the Neuque n Basin, Argentina. In: Tankard, A.J., Sua rez Soruco, R.,
1210 Welsink, H.J. (Eds.), Petroleum Basins of South America, American Association of Petroleum
1211 Geologists Memoirs, 62, pp. 383-402.
1212 Wilde, P., Lyons, T.W., Quinby-Hunt, M.S., 2004. Organic carbon proxies in black shales:
1213 molybdenum. Chemical Geology 206, 167-176.

1214 Witt, M.L.I., Mather, T.A., Pyle, D.M., Aiuppa, A., Bagnato, E., Tsanev, V.I., 2008. Mercury and
1215 halogen emissions from Masaya and Telica volcanoes, Nicaragua. Journal of Geophysical Research,
1216 Solid Earth 113, B06203. http://dx.doi.org/ 10.1029/2007JB005401.
1217 Zambardi, T., Sonke, J.E., Toutain, J.P., Sortinob, F., Shinoharac, H., 2009. Mercury emissions and
1218 stable isotopic compositions at Vulcano Island (Italy). Earth and Planetary Science Letters 277, 236-
1219 243.

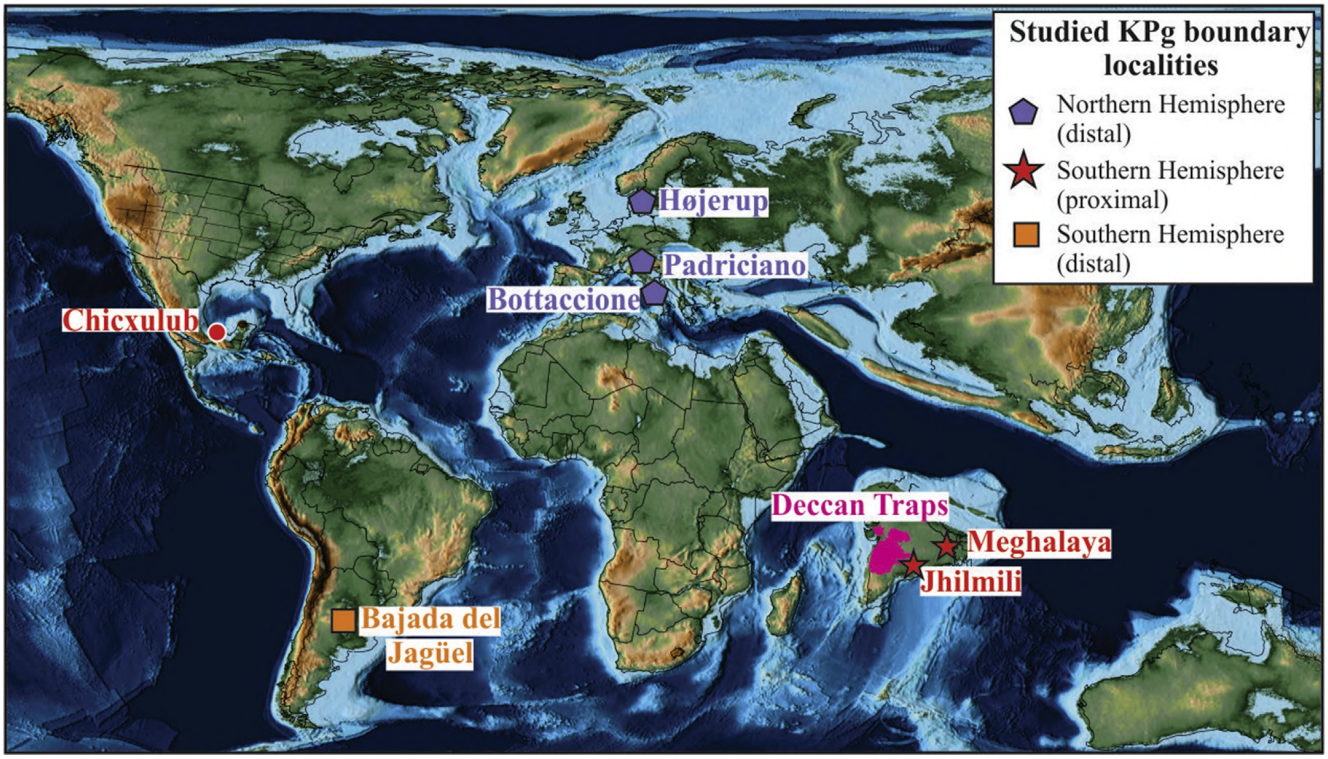

Fig. 1. Paleomap at 66 Ma showing paleogeography and location of the studied KPg boundary sections (based on Scotese, 2013). The location of the Chicxulub impact structure is indicated. Colored stars mark the three distinct types of studied KPg boundary sections in relation to the Deccan volcanic province center: (A) Northern Hemisphere (distal >5000 km); yellow; (B) Southern Hemisphere (proximal to very proximal; up to 1000 km); red; (C) Southern Hemisphere (distal > 5000 km); orange. (For interpretation of the references to color in this figure legend, the reader is referred to the web version of this article.)

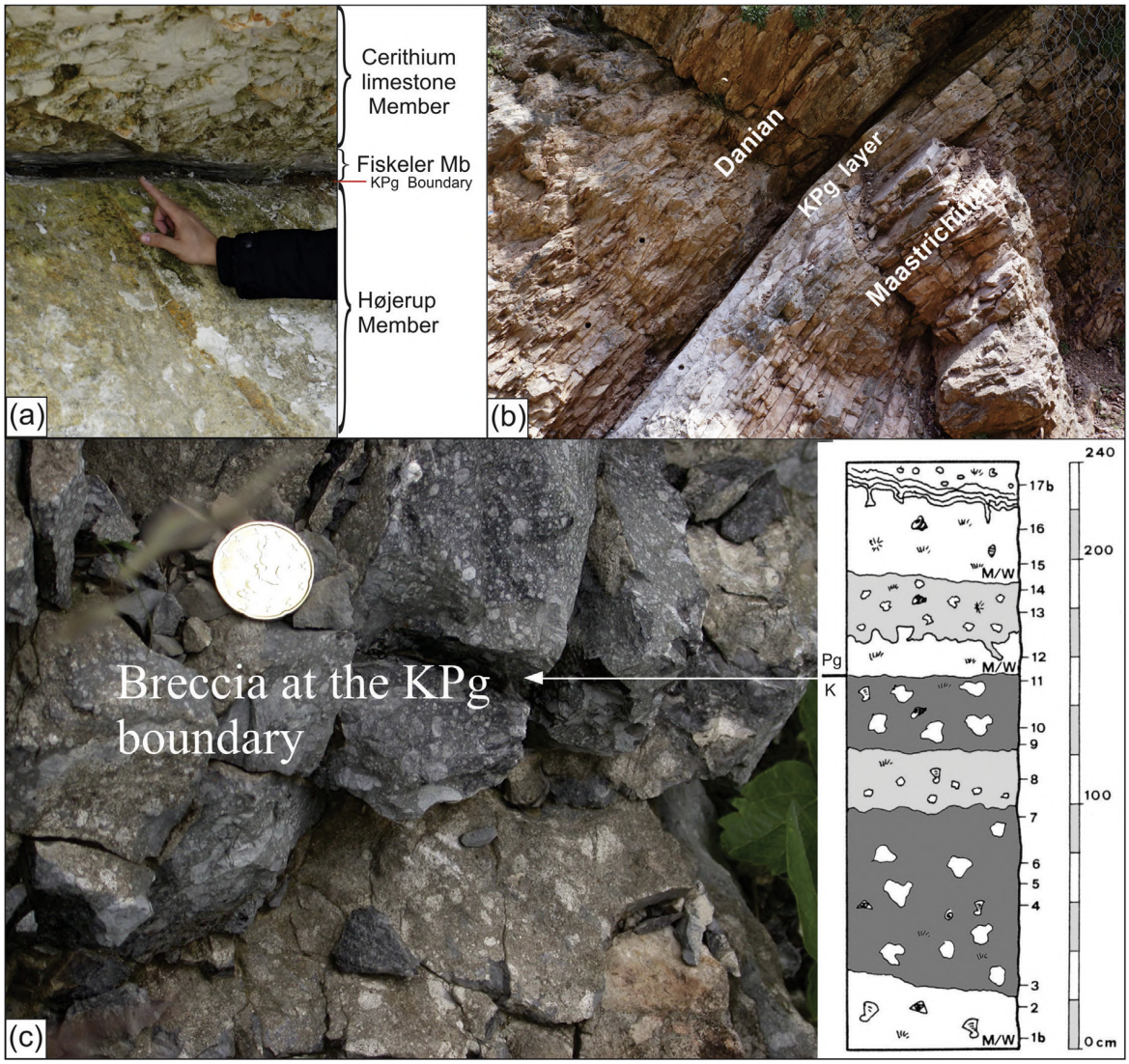

Fig. 2. (A) Closer view of the KPg boundary layer (Fiskeler Member) in the Højerup section, Stevns Klint, Denmark; (B) KPg boundary layer (1–2 cm thick) within the Scaglia Rossa Formation at the Bottaccione Gorge, near Gubbio, Italy; (C) Closer view of the upper breccia level at the KPg boundary in Padriciano, near Trieste, Italy.

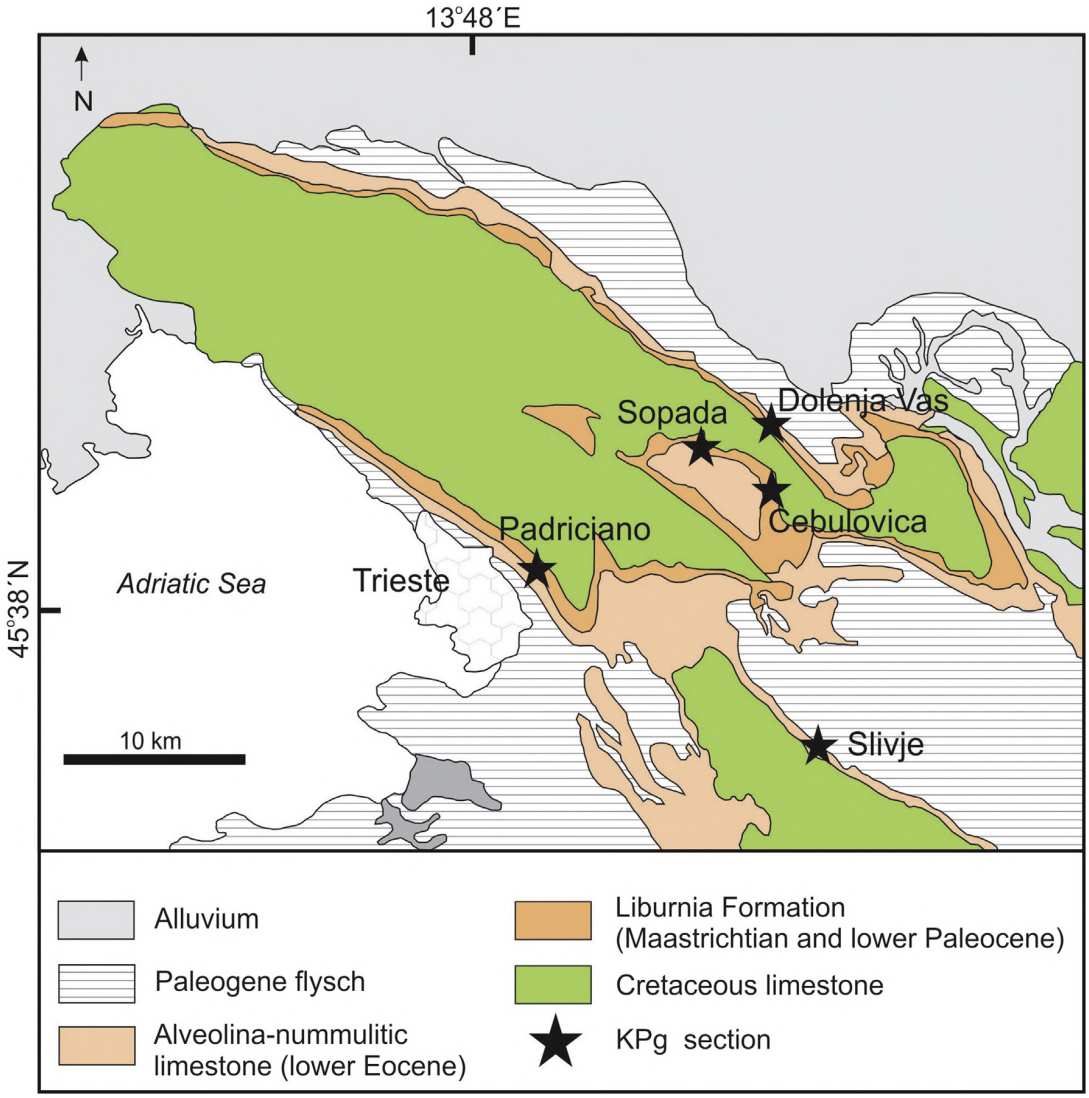

Fig. 3. Summary geological map showing five sites of studied KPg boundary sections in the Trieste Karst region of Slovenia and northeastern Italy (modified from Pugliese et al., 1995). Black stars mark the location of KPg boundary sections.

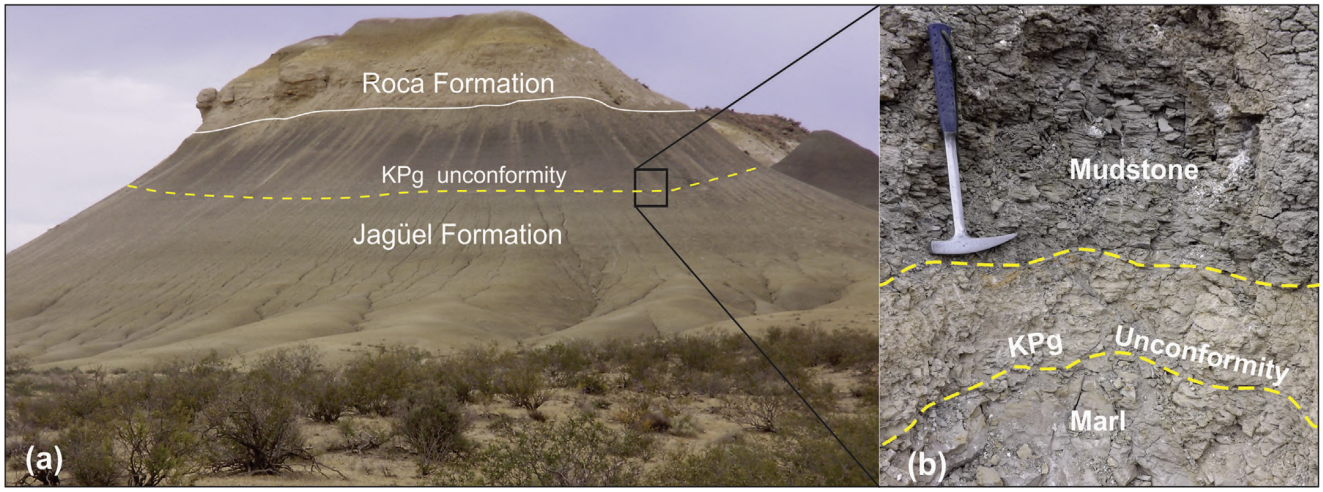

Fig. 4. Yellow volcanoclastic sandstone layer (20 cm thick) marking the KPg boundary in the Bajada del Jagüel section, Neuquén Basin, Argentina. (For interpretation of the references to color in this figure legend, the reader is referred to the web version of this article.)

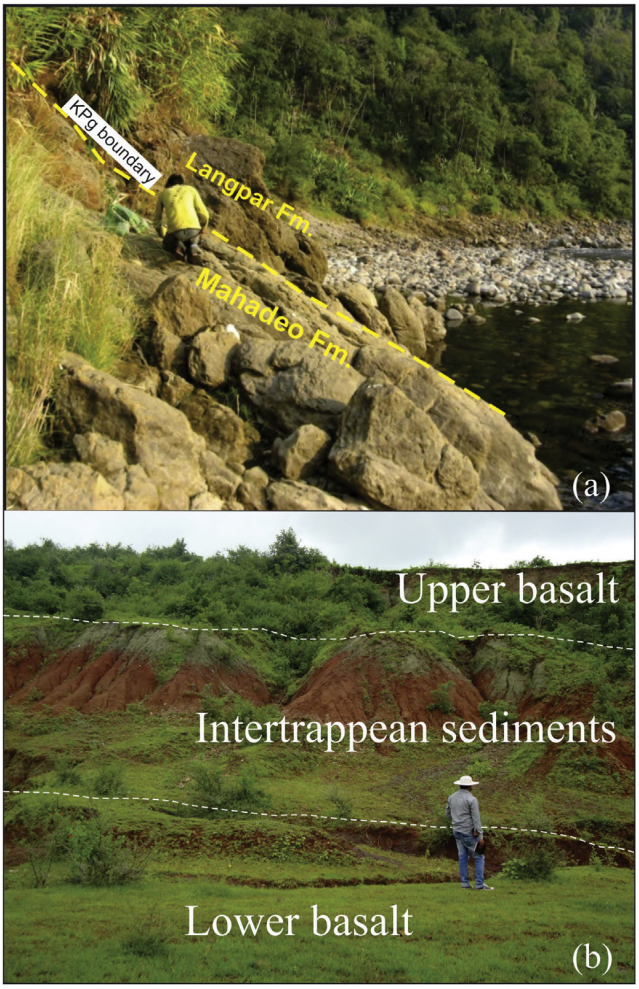

Fig. 5. Field aspects of the two sampled sections in India: (A) KPg boundary location between the Mahadeo and Langpar formations in an Um Sohrynkew River section, not far from Theria village, Shillong Plateau, northeastern India; (B) Jhilmili section showing the two basalt traps and sandwiched intertrappean sedimentary rocks.

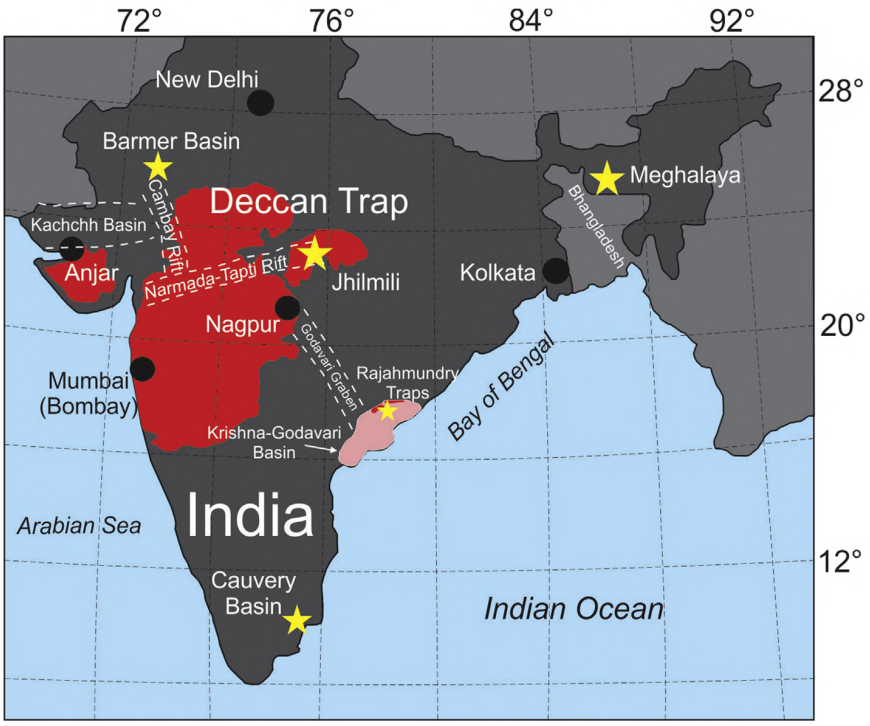

Fig. 6. Geographic map of India showing the location of well-known KPg boundary sections, marked by stars (Meghalaya, Jhilmili, Anjar, and Barmer, Krishna–Godavari and Cauvery basins). Also shown in this map is the Deccan volcanic province and the extent of the Narmada–Tapti seaway (modified from Cripps, 2002; Shukla and Srivastava, 2008; Keller et al., 2009).

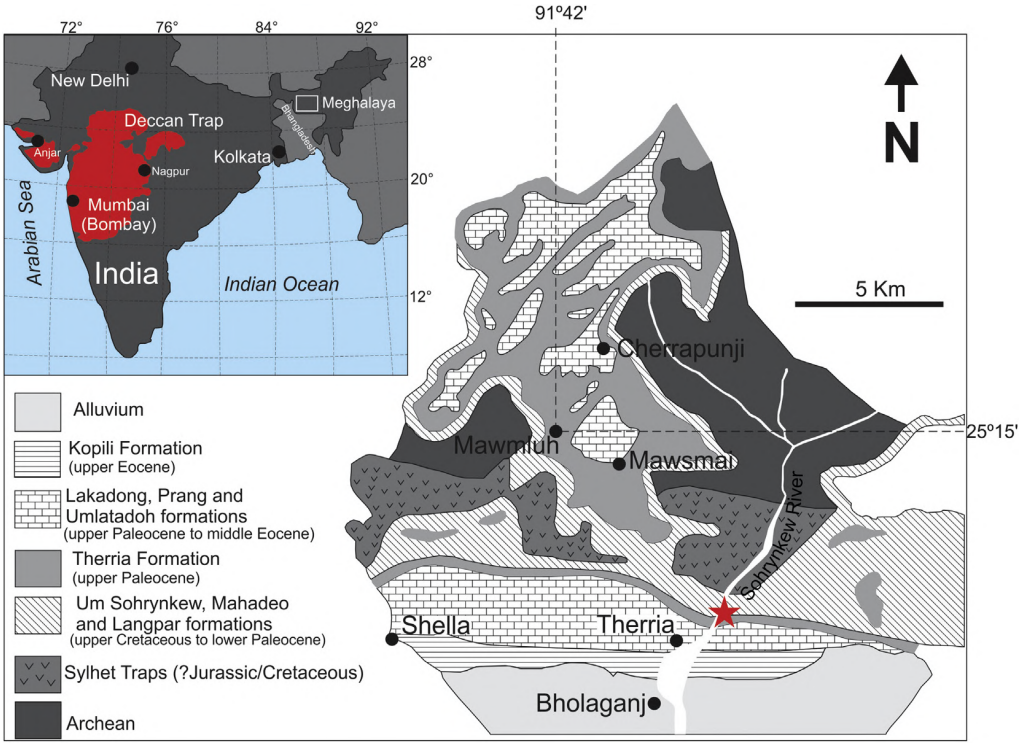

Fig. 7. Summary geological map of South Shillong Plateau, Meghalaya, northeastern India (modified from Tewari et al., 2010a, 2010b). Star indicates locality of the sampled section.

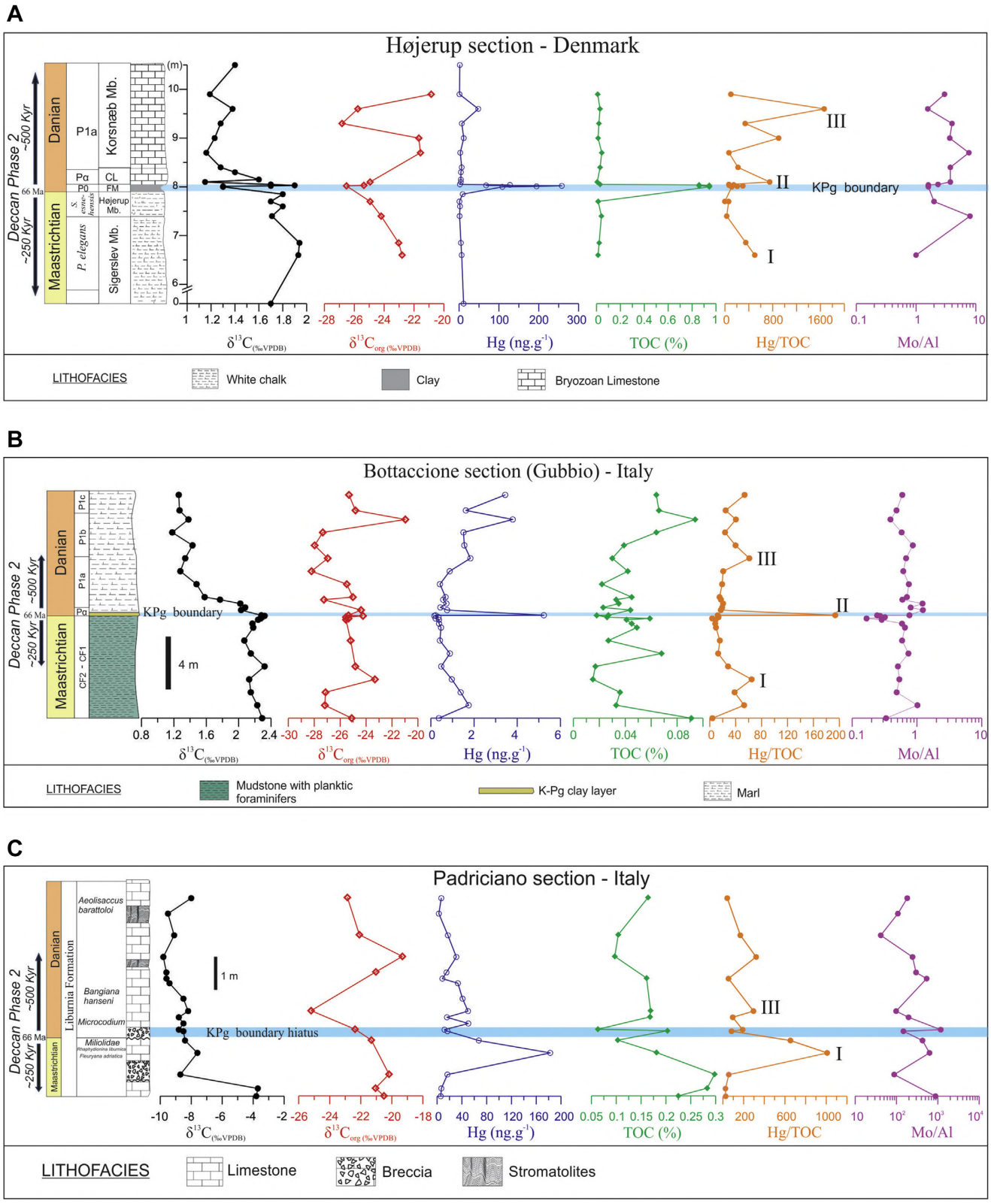

Fig. 8. (A) $\delta^{13}C_{carb}$, $\delta^{13}C_{org}$, Hg/TOC and Mo/Al variation patterns across the KPg boundary at Højerup, Stevns Klint (Maastrichtian planktic foraminiferal biostratigraphy from Surlyk et al., 2006, and Danian, from Rasmussen et al., 2005); (B) Bottaccione (Gubbio) section (planktic foraminiferal biostratigraphy from Coccioni et al., 2010; Coccioni and Premoli Silva, 2015) and (C) Padriciano section (foraminiferal biostratigraphy from Tewari et al., 2007), Italy.

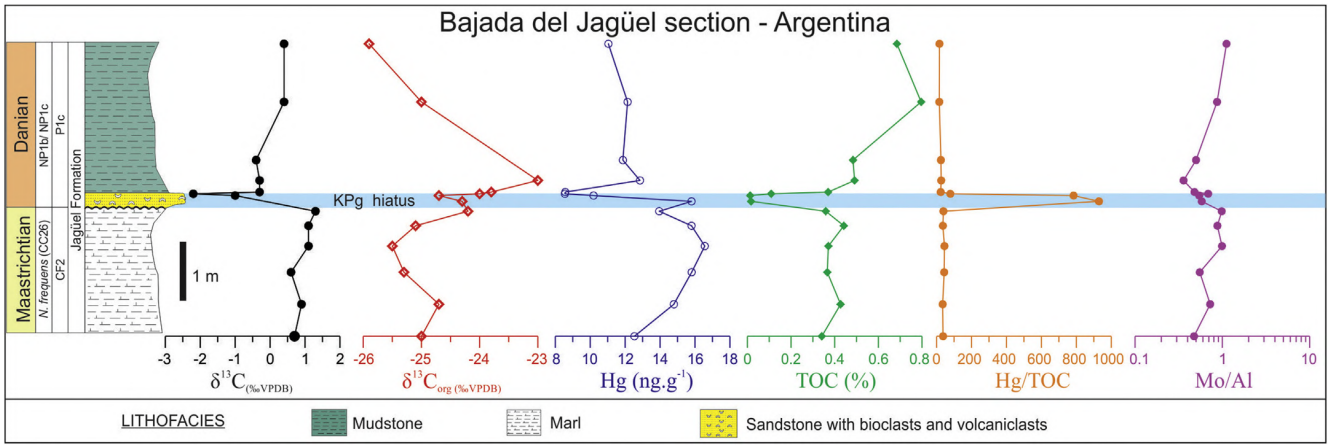

Fig. 9. $\delta^{13}C_{carb}$, $\delta^{13}C_{org}$, Hg/TOC and Mo/Al variation patterns across the KPg boundary in a section at Bajada del Jagüel, Neuquén Basin, Argentina (biostratigraphy according to Keller et al., 2007).

Table 1
C and O isotopes (‰ VPDB), total organic carbon (TOC %) and Hg ($ng \cdot g^{-1}$) across the KPg boundary in sections at Højerup (Denmark), and Bottaccione and Padriciano (Italy).

(a) Højerup section, Stevns Klint, Denmark

Formation	Member	Sample	Height (cm)	$\delta^{13}C$ ‰ VPDB	$\delta^{13}C_{org}$ ‰ VPDB	Hg ($ng \cdot g^{-1}$)	TOC(%)	Hg/TOC	Mo (ppm)	Al (%)	Mo/Al
Danian	Korsnæb Member	SKc	1050	1.4	–	1.8	–	–	–	–	–
Stevns Klint Formation		N7	990	1.19	−20.85	1.0	0.010	100.0	0.06	0.02	3.00
		N6	960	1.38	−25.76	48.2	0.029	1662.06	0.11	0.07	1.57
		N5	930	1.28	−26.82	6.8	0.020	340.00	0.08	0.02	4.00
		N4	900	1.23	−21.68	11.7	0.013	900.00	0.11	0.03	3.66
		N3	870	1.16	−21.57	3.0	0.044	68.18	0.23	0.03	7.66
		N2	840	1.28	–	6.6	0.030	220.00	0.15	0.04	3.75
Danian	Cerithium Limestone Member	D3	830	1.4	–	4.55	–	–	–	–	–
Rødvig Formation		D2	815	1.6	–	4.51	–	–	–	–	–
		N1	810	1.15	−24.94	4.5	0.006	750.00	0.15	0.04	3.75
		No. 3	805	1.7	–	2	0.030	66.66	0.14	0.06	2.33
	Fiskeler Member (KPg boundary)	FC-1	804	–	–	127.72	0.859	148.68	1.83	1.14	1.60
		FCD	803	1.9	−25.36	67.9	0.944	71.92	3.67	2.28	1.60
		FCC	802	1.7	−26.52	257.94	0.859	300.27	3.67	2.28	1.60
		FCB	801	1.3	–	194.53	0.944	206.06	3.67	2.28	1.60
		FCA	800	1.3	–	108.76	0.944	115.21	3.67	2.28	1.60
Maastrichtian	Højerup Member (gray chalk)	M2	785	1.8	–	9.09	–	–	–	–	–
Møns Klint Formation		N (−1)	770	0.71	−24.94	–	0.014	–	0.02	0.01	2.00
		M1A	770	1.7	–	0.88	0.014	62.85	0.02	0.01	2.00
		No. 2	760	1.8	–	2.3	–	–	–	–	–
		N (−2)	740	1.71	−24.20	<1.26	0.041	30.73	0.08	0.01	8.00
		N (−3)	685	1.94	−23.03	4.6	–	–	–	–	–
		N (−4)	660	1.93	−22.80	6.5	0.015	433.3	0.01	0.01	1.00
	Sigerslev Member (white chalk)	No. 1	0	1.7	–	11.3	–	–	–	–	–

(b) Bottaccione section, Italy

Lithology	Sample	Height (cm)	$\delta^{13}C_{carb}$ ‰ VPDB	$\delta^{13}C_{org}$ ‰ VPDB	Hg ($ng \cdot g^{-1}$)	TOC (%)	Hg/TOC	Mo (ppm)	Al (%)	Mo/Al
Marl	GP-28	1685.4	1.26	−25.32	3.44	0.064	53.75	0.19	0.32	0.59
	GP-27	1565.4	1.27	−24.82	1.62	0.066	24.54	0.15	0.31	0.48
	GP-26	1495.4	1.38	−20.97	3.79	0.094	40.31	0.16	0.41	0.39
	GP-25	1395.4	1.18	−27.34	1.51	0.064	23.59	0.18	0.31	0.58
	GP-24	1295.4	1.43	−27.97	1.55	0.039	39.74	0.19	0.22	0.86
	GP-23	1195.4	1.34	−26.96	1.83	0.030	61.00	0.17	0.25	0.68
	GP-22	1095.4	1.28	−28.21	0.87	0.042	20.71	0.24	0.39	0.61
	GP-21	995.4	1.48	−25.49	0.42	0.022	19.09	0.15	0.20	0.75
	GP-20	895.4	1.58	−25.02	0.68	0.045	15.11	0.21	0.30	0.70
Marl (rhytmites; carbonate production decreases in the Danian)	GP-19	875.4	1.77	−27.25	0.57	0.033	17.27	0.34	0.57	0.91
	GP-18	845.4	2.02	–	0.72	0.035	20.57	0.39	0.32	1.21
	GP-17	815.4	2.08	–	0.44	0.023	19.13	0.12	0.15	0.80
	GP-16	795.4	2.03	−24.39	0.75	0.044	17.04	0.21	0.17	1.23
Greenish brown clay layer	GP-15	(KPg boundary layer)	−26.78		5.23	0.027	193.70	0.49	0.64	0.29
Mudstone with planktic foraminifera	GP-14	794	2.28	−25.36	0.22	0.018	12.22	0.09	0.37	2.67
	GP-13	790	2.32	−24.24	0.16	–	–	0.07	0.26	0.26
	GP-12	780	2.29	−25.55	0.35	0.026	13.46	0.08	0.25	0.32
	GP-11	770	2.27	−25.35	0.22	0.059	3.72	0.05	0.30	0.16
	GP-10	760	2.24	−25.55	0.37	0.041	9.02	0.06	0.21	0.28
	GP-9	730	2.17	–	0.38	0.045	8.44	0.20	0.34	0.58
	GP-8	700	2.18	–	0.47	0.049	9.59	0.17	0.26	0.65
	GP-7	600	2.07	−25.19	0.42	0.027	15.55	0.23	0.39	0.58
	GP-6	500	2.15	–	0.88	0.068	12.94	0.17	0.23	0.73
	GP-5	400	2.32	−24.83	0.48	0.017	28.23	0.30	0.59	0.50
	GP-4	300	2.13	−23.32	0.97	0.015	64.66	0.23	0.43	0.53
	GP-3	200	2.15	−27.13	1.38	0.036	38.33	0.18	0.37	0.48
	GP-2	100	2.23	−27.18	1.75	0.033	53.03	0.58	0.57	1.01
	GP-1	0	2.29	−25.11	0.37	0.091	4.06	0.26	0.78	0.33

(c) Padriciano section, Italy

Stage	Formation	Sample	Height (m)	$\delta^{13}C$ ‰ VPDB	$\delta^{13}Corg$ ‰ VPDB	Hg $ng \cdot g^{-1}$	TOC (%)	Hg/TOC	Mo (ppm)	Al (%)	Mo/Al
Danian	Liburnia	VT 16	6.4	−8.0	−22.86	6.8	0.164	41.46	1.82	0.01	182
		VT 15	5.9	−9.5	–	2.9	–	–	1.08	0.01	108
		VT 14	5.2	−9.1	−22.09	17.5	0.104	168.26	3.33	0.08	41.62
		VT 13	4.5	−9.8	−19.32	31.1	0.097	320.61	4.89	0.02	244.50
		VT 12	4	−9.6	−21.03	15.2	–	–	2.97	0.01	297
		VT 11	3.8	−9.6	–	8.6	0.161	53.41	5.36	0.01	536
		VT 10	3.65	−9.4	–	33.6	–	–	–	–	–
		VT 9	3.15	−8.5	–	41.2	–	–	–	–	–
		VT 8	2.75	−8.2	−25.20	49.9	0.169	295.26	1.96	0.02	98.00
		VT 7	2.55	−8.8	–	15.9	0.168	94.64	1.96	0.01	196
		VT 6	2.35	−8.5	–	50.5	–	–	–	–	–
		VT 5	2.15	−8.8	−22.37	12.0	0.063	190.47	11.79	0.01	1179.00

(*continued on next page*)

Table 1 (*continued*)

(c) Padriciano section, Italy

Stage	Formation	Sample	Height (m)	δ^{13}C ‰ VPDB	δ^{13}Corg ‰ VPDB	Hg ng·g^{-1}	TOC (%)	Hg/TOC	Mo (ppm)	Al (%)	Mo/Al
KPg boundary		KPg breccia	2.1	−8.5	–	16.8	0.203	82.75	1.47	0.01	147
Maastrichtian		VT 4	1.8	−8.4	−21.32	67.3	0.103	653.39	8.52	0.02	426.00
		VT 3	1.4	−7.6	–	182.5	0.181	1008.28	25.16	0.04	629.00
		VT 2	0.7	−8.7	−20.18	16.7	0.298	56.04	0.88	0.01	88
		VT 1	0.25	−3.7	−21.05	6.9	0.283	24.38	1.17	0.00	0
		VT 0	0	−3.8	−20.51	5.9	0.225	26.22	8.76	0.01	876

Table 2
C- and O-isotope analyses (‰ VPDB), total organic carbon (TOC, %), Hg ($ng \cdot g^{-1}$), Mo (ppm) and Al (%) in a KPg section at Bajada del Jagüel, Argentina.

(a) Bajada del Jagüel section, Neuquén Basin, Argentina

Formation	Lithology	Sample	Height (m)	$\delta^{13}C_{‰\ VPDB}$	$\delta^{13}C_{org\ ‰\ VPDB}$	Hg ($ng \cdot g^{-1}$)	TOC (%)	Hg/TOC	Mo (ppm)	Al (%)	Mo/Al
Jagüel Formation	Mudstone	KT 12	5.03	0.4	−25.9	11.04	0.685	16.11	1.92	1.72	1.11
		KT 11	4.03	0.4	−25.0	12.14	0.796	15.25	1.07	1.23	0.86
		KT10	3.03	−0.4	–	11.87	0.484	24.52	0.78	1.56	0.50
		KT9	2.68	−0.3	−23.0	12.85	0.491	26.17	0.55	1.53	0.35
		KT 8	2.48	−0.3	−23.8	8.57	0.370	23.16	0.61	1.27	0.48
	Sandstone with bioclasts and volcaniclasts	KT7	2.45	−2.2	−24.0	8.55	0.109	78.44	0.75	1.09	0.68
		KT 6	2.42	−1	−24.7	10.19	0.013	783.84	0.57	1.05	0.54
		KT 5	2.32	−0.6	−24.3	15.80	0.017	929.41	0.75	1.29	0.58
	Marl	KT 4	2.15	1.3	−24.2	13.95	0.359	38.85	1.17	1.19	0.98
		KT 3	1.9	1.1	−25.1	15.8	0.442	35.74	1.36	1.55	0.87
		KT 2	1.55	1.1	−25.5	16.56	0.371	44.63	1.09	1.10	0.99
		KT 1	1.1	0.6	−25.3	15.81	0.366	43.19	0.59	1.07	0.55
		KT0	0.55	0.9	−24.7	14.79	0.427	34.63	0.74	1.02	0.72
		KT (-1)	0	0.7	−25.0	12.53	0.341	36.74	0.56	1.18	0.47

Table 3
C- and O-isotope analyses (‰ VPDB, %), total organic carbon (TOC, %), and Hg ($ng \cdot g^{-1}$) in samples from India.

(a) Meghalaya section, Um Sohrynkew, northeastern India.

Formation	Lithology	Sample	Height (cm)	$\delta^{13}C$ ‰ $_{VPDB}$	$\delta^{13}C_{org}$ ‰ $_{VPDB}$	Hg ng$\cdot g^{-1}$	TOC (%)	Hg/TOC	Mo (ppm)	Al (%)	Mo/Al
Langpar (Danian)	Light gray shale	KT 25	10	0.1	−23.78	10.3	0.042	245.23	–	–	–
	Dark gray shale	KT 24	10	1.1	−25.36	9.8	0.039	251.28	–	–	–
		KT 23	10	0.4	−24.96	7.4	0.040	185.00	–	–	–
		KT 22	10	0.6	−24.35	11.5	0.039	294.87	–	–	–
		KT 21	10	−0.1	−24.93	2.4	0.042	57.14	–	–	–
		KT 20	10	0.4	−24.91	7.8	0.036	216.66	–	–	–
		KT 19	10	−0.1	−24.42	3.9	0.044	88.63	–	–	
		KT 18	10	−0.1	−24.43	12.1	0.041	295.12	–	–	–
		KT 17	10	0.6	−24.38	6.2	0.065	95.38	–	–	–
		KT 16	10	1.3	−24.59	6.7	0.039	171.79	–	–	–
		KT 15	10	1.4	−24.79	10.0	0.035	285.71	–	–	–
		KT 14	10	1.1	−24.77	11.8	0.033	357.57	–	–	–
		KT 13	10	−0.0	−24.49	4.3	0.039	110.25	–	–	–
		KT 12	10	−0.1	−24.56	1.6	0.627	2.55	2.05	1.13	1.81
	Light gray shale	KT 11	10	0.1	−21.69	2.8	0.571	4.90	2.93	1.05	2.79
		KT 10	10	0.1	−21.99	0.0	0.447	0.00	0.71	1.39	0.51
		KT 9	10	0.5	−20.22	0.0	0.468	0.00	0.53	1.16	0.45
KPg boundary layer	Yellowish brown to reddish layer	KPg bulk	10	−8.13	−23.12	6.3	0.059	16.94	3.11	1.81	1.71
Mahadeo (Maastrichtian)	Greenish sandstone and shale	KT8	10	−0.4	−23.93	6.3	–	–	–	–	–
		KT7	10	0.4	−23.91	3.2	–	–	–	–	–
		KT6	10	−0.0	−23.91	6.2	0.070	88.57	0.66	1.50	0.44
		KT5	10	0.7	−24.14	2.9	0.052	55.76	0.59	1.45	0.40
		KT4	10	0.2	−24.82	13.1	0.335	39.10	1.67	1.22	1.36
		KT3	10	0.5	−23.81	98.6	0.424	232.54	1.21	1.53	0.79
		KT2	10	0.3	−24.49	31.4	0.337	93.17	1.88	1.18	1.59
		KT1	10	1.0	−24.54	6.9	0.349	19.77	0.91	1.12	0.81

(b) Jhilmili Section, central India

	Lithology	Sample	Height (m)	$\delta^{13}C$ ‰ $_{VPDB}$	$\delta^{13}C_{org}$ ‰ $_{VPDB}$	Hg ng$\cdot g^{-1}$	TOC (%)	Hg/TOC	Mo (ppm)	Al (%)	Mo/Al
Upper Basalt Trap	2.5 m thick basaltic flow	JMR 20	0.5	–	−20.73	12.4	0.030	413.33	0.13	2.14	0.060
Paleosol Section (Danian)	Greenish clay layer with calcitic veins	JMR 19	0.3	−3.7	−28.27	15.3	0.093	164.51	0.07	1.97	0.035
		JMR 18	0.5	−5.6	−25.44	12.3	0.060	205.00	0.04	1.74	0.022
	Soft ferricrete fine-grained, brick red with yellowish tint	JMR 17	0.5	−3.3	−20.73	8.7	0.041	212.19	0.03	3.73	0.008
		JMR 16	0.5	−2.6	−23.33	100.2	0.032	3131.25	0.01	2.29	0.004
		JMR 15	0.5	−2.6	–	19.2	0.036	533.33	0.01	2.21	0.004
		JMR 14	0.5	−3.20	−24.45	9.9	0.024	412.50	0.03	2.22	0.013
	Claystone with laminar features, grayish brown in color, relatively harder	JMR 13	0.3	−3.5	−25.53	17.7	0.067	264.17	0.07	2.29	0.030
		JMR 12	0.4	−3.3	−24.92	6.2	0.045	137.77	0.64	2.62	0.244
		JMR 11	0.6	−4.7	−23.26	14.8	0.078	189.74	1.68	1.65	1.018
	Soft ferricrete, fine- grained, brick red with yellowish tint	JMR 10	0.3	−4.1	–	51.8	0.039	1328.20	0.36	3.07	0.117
		JMR 09	0.3	−6.0	−23.38	14.5	0.035	414.28	0.82	2.49	0.329
		JMR 08	0.3	−8.0	−25.31	11.8	0.056	210.71	0.07	3.94	0.017
		JMR 07	0.5	–	−20.33	19.0	0.062	306.45	0.05	3.79	0.013
	Hard sediment layer within the paleosol with clasitc grains with calcitic cement	JMR 06	0.3	−11.0	−24.68	14.5	0.053	273.58	0.60	2.03	0.295
		JMR 05	0.5	−12.1	−24.41	24.1	0.074	325.67	0.04	3.56	0.011
	Lowest layer of paleosol ferricrete with calcitic veins	JMR 04	0.5	−3.4	−24.43	20.7	0.046	450.00	0.28	2.71	0.103
		JMR 03	0.5	−9.9	−22.97	11.8	0.084	140.47	0.03	3.88	0.007
Lower Basalt Trap	2.0 m thick basaltic flow	JMR 02	0	–	–	–	0.071	–	0.04	1.48	0.027

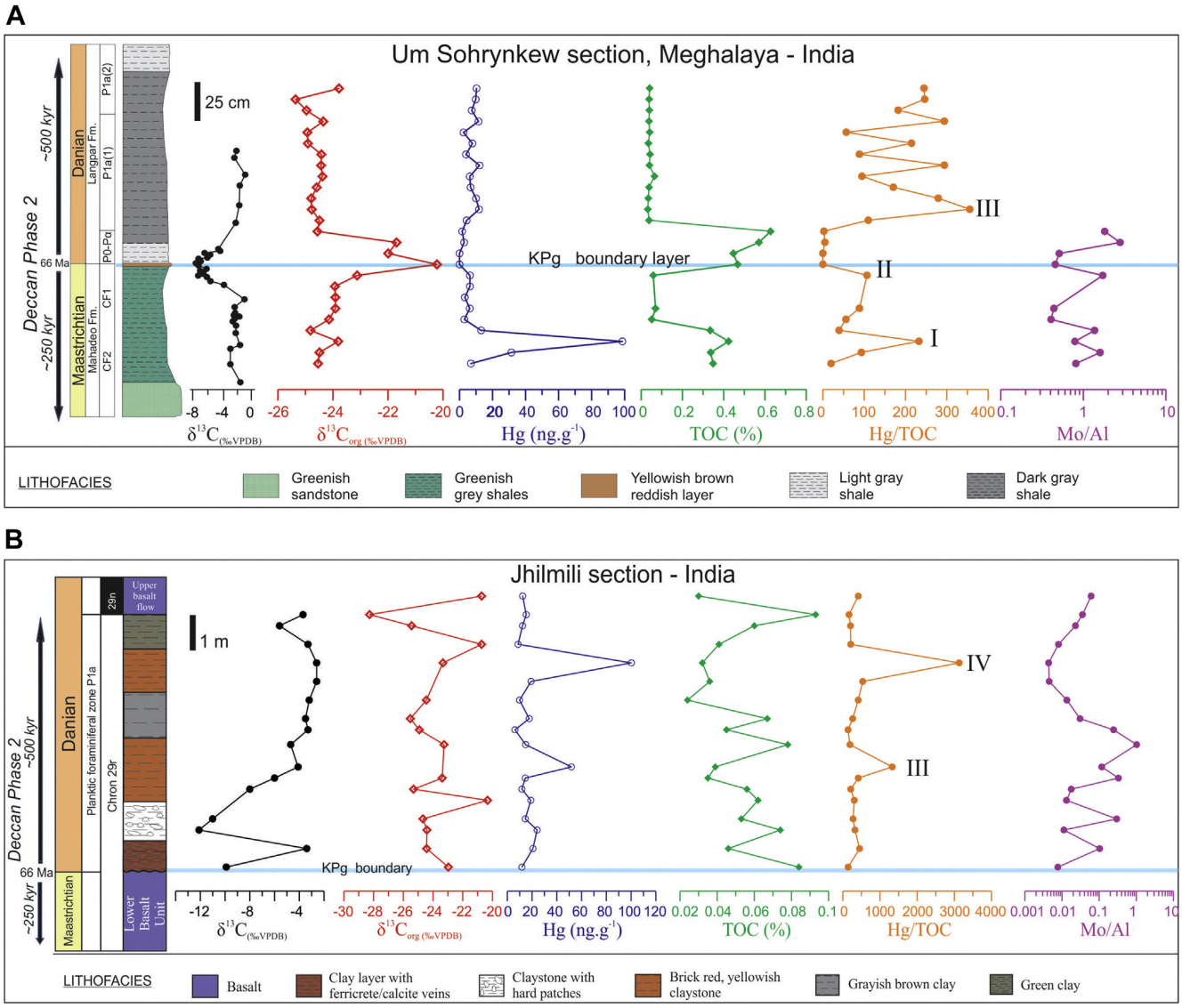

Fig. 10. $\delta^{13}C_{carb}$, $\delta^{13}C_{org}$, Hg/TOC and Mo/Al variation patterns across the KPg boundary at: (A) Um Sohrynkew River section (Meghalaya), south Shillong Plateau, northeastern India ($\delta^{13}C_{carb}$ from Gertsch et al., 2011; planktic foraminifera biostratigraphy from Mukhopadhyay, 2008; Pal et al., 2015) and (B) Jhilmili section, Madhya Pradesh, central India (planktic foraminiferal biostratigraphy from Keller et al., 2009).

Table 4
Hg isotopes (‰ relative to NIST SRM 3133) in samples with Hg enrichments: spike I (Meghalaya, Padriciano); spike II (Højerup, Bottaccione, Meghalaya), and Bidart (France; for comparison); spike III (Jhilmili), besides samples from across the KPg boundary at Bajada del Jagüel.

Samples	δ^{199}Hg	δ^{200}Hg	δ^{201}Hg	δ^{202}Hg	Δ^{199}Hg	Δ^{200}Hg	Δ^{201}Hg
Mass dependent fractionation (MDF)					Mass independent fractionation (MIF)		
(a) Fiskeler Member (KPg boundary layer), Denmark							
FCA	−0.51	−1.06	−1.76	−2.34	0.08	0.11	−0.01
FCB	−0.28	−0.74	−1.18	−1.62	0.13	0.07	0.04
FCC	−0.29	−0.55	−0.86	−1.06	−0.02	−0.02	−0.06
FCD	−0.43	−0.92	−1.44	−1.93	0.06	0.05	0.01
(b) Bottaccione, Italy (KPg boundary layer)							
GP-15	−0.26	−0.59	−0.93	−1.28	0.06	0.05	0.03
(c) Meghalaya, India							
KT-3	−0.35	−0.78	−1.16	−1.61	0.06	0.03	0.05
KT-bulk	−0.64	−0.94	−1.58	−1.89	−0.16	0.01	−0.16
(d) Jhilmili, India							
JM-16	−0.60	−0.57	−0.98	−1.01	−0.34	−0.06	−0.22
JM-10	−1.01	−1.12	−1.92	−2.18	−0.46	−0.02	−0.28
(e) Padriciano, Italy							
VT-3	−0.08	−0.69	−1.00	−1.38	0.27	0.00	0.04
(f) Jagüel Formation, Neuquén Basin, Argentina							
K-T-12	0.07	−0.29	−0.29	−0.62	0.22	0.02	0.18
K-T-11	−0.08	−0.67	−0.89	−1.41	0.27	0.04	0.17
K-T-10	−0.14	−0.59	−0.77	−1.17	0.16	−0.01	0.10
K-T-9	−0.13	−0.59	−0.76	−1.18	0.17	0.00	0.13
K-T-8	−0.06	−0.59	−0.74	−1.15	0.13	−0.01	0.12
K-T-7	−0.08	−0.52	−0.68	−1.00	0.17	−0.02	0.08
K-T-6	−0.10	−0.48	−0.61	−0.87	0.12	−0.05	0.04
K-T-5 (KPg layer)	−0.14	−0.57	−0.73	−1.05	0.13	−0.05	0.06
K-T-4	−0.03	−0.36	−0.49	−0.77	0.17	0.02	0.09
K-T-3	−0.12	−0.60	−0.88	−1.27	0.20	0.04	0.07
K-T-2	−016	−0.61	−0.84	−1.22	0.15	0.01	0.08
K-T-1	−0.12	−0.50	−0.68	−1.04	0.14	0.02	0.10
(g) Bidart, France							
KPg boundary layer	−0.04	−0.34	−0.42	−0.74	−1.12	−0.15	0.03
BI-9.28.5	−0.11	−0.57	−0.66	−1.44	−1.56	0.25	0.15
BI-9.34.2	0.05	−0.11	−0.13	−0.31	−0.73	0.12	0.04
BI-9.36.2	0.08	−0.10	−0.07	−0.25	−0.61	0.15	0.03
BI-10.35.1	−0.33	−1.28	−1.68	−2.66	−4.30	0.33	0.06
BI-11.7.3	0.13	−0.16	−0.04	−0.66	−0.73	0.30	0.17

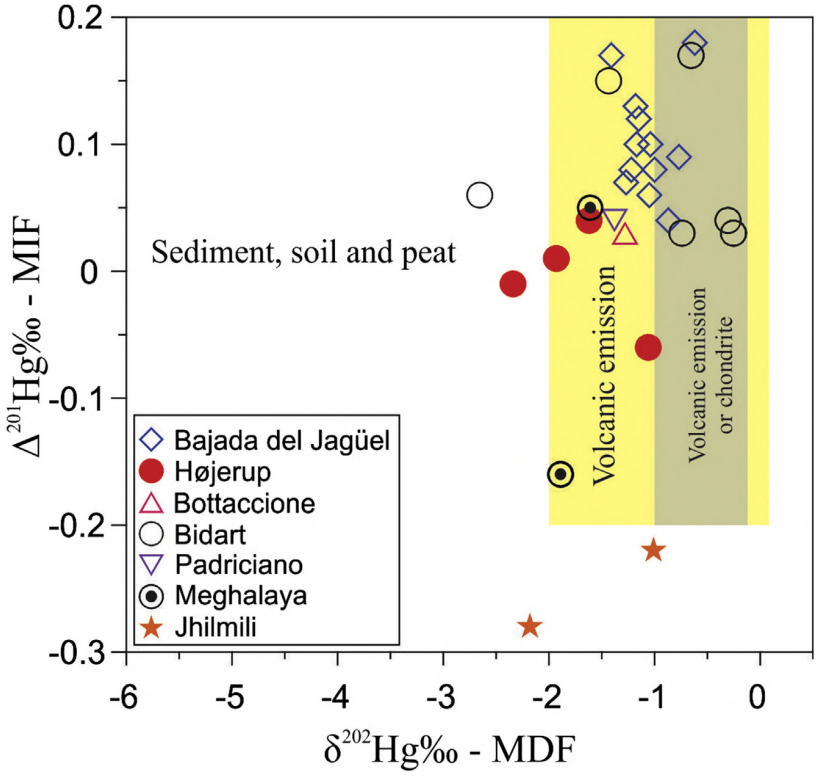

Fig. 11. In a δ^{202}Hg (MDF)–Δ^{201}Hg (MIF) plot, values most samples in this study lie within the range for volcanogenic Hg. Ranges for volcanogenic and chondritic Hg are from Bergquist and Blum (2009) and are shown as vertical bars.